Aalto University
School of Chemical
Engineering

Nguyen Hoang Vu

DESIGN, ASSEMBLY AND CHARACTERIZATION OF HIGHLY CURVED DNA ORIGAMI STRUCTURES

Master´s Programme in Life Science Technologies
Major in Biosystems and Biomaterials Engineering

Master's thesis for the degree of Master of Science in Technology
submitted for inspection, Espoo, 29 Nov, 2018.

Supervisor	Professor Anton Kuzyk
Instructor	Dr. Nguyen Minh Kha

Author Nguyen Hoang Vu

Title of thesis Design, assembly and characterization of highly curved DNA origami structures

Degree Programme Life Science Technologies

Major Biosystems and Biomaterials Engineering

Thesis supervisor Professor Anton Kuzyk

Thesis advisor(s) / Thesis examiner(s) Dr. Nguyen Minh-Kha

Date 29.11.2018 **Number of pages** 47+ 4 **Language** English

Abstract

DNA origami technique has found application in building nanoscale structures of various complexity and shape, including 3D curvatures with diameters as small as 25 nm, which opens up new venue of research including mimicking cellular components like nuclear pore complex. However, currently there is no concrete guideline available to build such 3D structures and researchers have to rely on an iterative design approach. Moreover, available curvatures in literature were all implemented based on a single type of helix packing, indicating certain difficulty in assemble curvature with the more densely packed square-lattice.

In this thesis, a set of principles previously described for curved single-layer structures were adapted for multilayer designs and validated with three structures different in cross-section, torsional rigidity, and dimension. The folding quality and structural integrity of each were characterized with gel electrophoresis and transmission electron microscopy. Comparison among three structures prove the improvement in building curvatures using the proposed principles and suggest the importance of torsional rigidity in designing curvatures. The effort to assemble a square-lattice-based structure meets limited success yet could be improved with further iterations.

Keywords DNA Nanotechnology, DNA origami, DNA curvature, DNA ring

Preface

I want to thank my supervisor Anton Kuzyk for the guidance and support that enable the better angels of my nature the space and time to grow, and the equanimity with which he put up with many of my mistakes and folly throughout our year-long journey.
Thanks to Kha, my advisor, for generally staying out of the way yet always within earshot, ready to be a personal counselor when needed, both academically and professionally.
Thanks to my family for the unwavering affection. And my dad, for the terrible cover-up enthusiastically put up to maintain my focus on the final step of this journey.
Finally, the biggest thanks are due to my partner, for lurking resolutely in the future and refusing to distract me from my study. All the more reason to conclude this chapter in a timely manner.

Otaniemi, 29.11.2018

Nguyen Hoang Vu

Contents

1 Introduction

It is a truth universally acknowledged, that a structure, irrespective of design, size, or elemental composition, must be either formed by stripping down the outer layer from the original block of material or assembled from the bottom up using constituent parts [1]. In the realm of nanotechnology research, the latter approach, with molecular self-assembly as a prime example, plays an increasingly important role in forming biologically relevant structures [2] due to the greater ease to control nanoscale features, an advantage that can only grow as understanding of molecular interactions deepens.

DNA origami is a technique within molecular self-assembly in which weak interactions between nucleotides, e.g. hydrogen bonds and van der Waals interactions, are employed to assemble DNA molecules into a particular structure. The most common and versatile method to build DNA origami structure, known as scaffolded DNA origami, utilizes a long single-stranded DNA, typically of less than 10,000 bases, called scaffold, and hundreds of shorter DNA oligonucleotides ranging from 20-60 bases in length [3], interweaving in a predefined manner to arrive at the final structure. The first proof of concept for DNA origami was demonstrated in a seminal paper by Paul Rothermund in 2006 in which he succeeded in assembling 2D structures with arbitrary patterns [4]. The paper broke the ground for further research by outlining the general principles of DNA origami design. Subsequently, constructing DNA origami structures was further facilitated by design and simulation applications, such as caDNAno and CanDo [5], [6]. CaDNAno, in particular, provides a framework for 3D DNA origami design with two types of helix packing known as honeycomb and square lattice.

Besides building particles of linear shape, DNA origami also demonstrated its applicability in forming curved structures, which opens up important research venues such as mimicking nuclear pore complex, the gatekeeper for nuclear transport in eukaryotic cells [7].

Curved DNA origami objects were first constructed in 2009 [8], when structures with varied degree of curvature and complexity were successfully assembled. Arguably, this pioneering research encounters some difficulties in assembling structures with small radius of curvature. Secondly, precise calculation for designing a certain degree

of curvature is lacking. The only paper that attempted to explain the design of curvatures using DNA origami was published by Dongran Han group in 2011 [9]. The proposed principles, however, were only implemented for single-layer structures, leaving open the question of whether those guidelines can be useful in 3D designs.

While an iterative design approach with the help of structure prediction software provides a viable alternative to design structure with desired degree of curvature, the resultant designs often contain significant internal tension which could hamper successful assembly. Additionally, for certain designs, prediction softwares simply could not resolve the internal tension and leave researchers with significant guesswork as to how their designs would turn out.

A survey of available literature shows that all current curvatures were built from honeycomb lattice, rather than square lattice [7], [8], [10]–[15]. Presumably, the denser helix packing and inherent twist of the latter are factors deterring researchers from building a curvature with square-lattice based cross-section. Nevertheless, an advantage of using such lattice over honeycomb is that it will allow for a greater range of possible interfaces [16]. The denser nature of square-latticed origami structures will also be beneficial in applications where a compact but rigid cross-section is preferable [16].

Thus, the goals of this thesis are to:

- Provide a calculation framework to design structure with arbitrary degree of curvature.
- Assemble 3D, DNA-origami-based, fully closed curvatures with either honeycomb or square lattice cross-section to validate the above framework.

Section 2 of this thesis provides an overview of how DNA origami makes use of DNA double helix natural conformation to assemble nanoscale objects, with special attention on curved structures. Section 3 describes materials and methods used in this thesis, followed by section 4, which reports results and discussion and section 5 for conclusion.

2 DNA as structural material

2.1 Structural properties of DNA

DNA is a polymer of deoxyribonucleotides which consist of a sugar, a phosphate group and a nitrogenous base. The basic building block of DNA are deoxyribonucleotide monomers, with four naturally occurring monomers differentiated by their nitrogenous base, including adenine (A), guanine (G), thymine (T), and cytosine (C) [17].

The primary structure of a DNA strand is defined as the linear sequence of nucleotides, while secondary structure includes information about the interactions between bases, which are predominantly hydrogen bonding and base stacking [18], [19]. From an energetic perspective, base stacking is the most important interaction in determining the conformation of a double helix, and the propensity towards forming a helix is due to the stacking of the individual bases [20]. Due to the different hydrophilicity of each component, the sugar and phosphate constitute the outer backbone of the double helix in a polar solvent while the interior shelters the water-insoluble and hydrophobic nitrogenous bases [20].

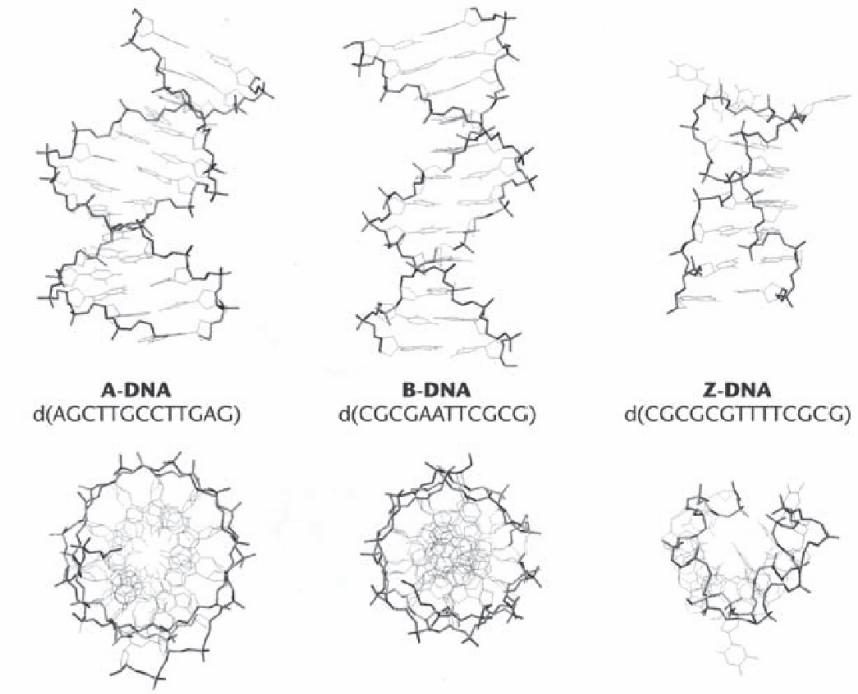

Figure 1. Three different conformations of DNA double helix with side views (top) and top views (bottom). Illustration adopted from [20].

When two complementary DNA strands intertwine, they could constitute various conformations differing in helix diameter, degree of twist and handedness [21]. The three most common forms of DNA double helices are A, B, and Z forms (Figure 1) [22].

Figure 2 illustrates the main feature of B-form DNA double helix, with the sugar-phosphate backbones interweaving at the surface of an imaginary tube while the nitrogenous bases pair to those of the opposite strand via hydrogen bonds. In the most common form of DNA double helix, B form, the distance between two adjacent bases in the same strand is 0.34 nm, with 10.5 bases completing a full turn. The diameter of the helix is 2 nm [23], [24].

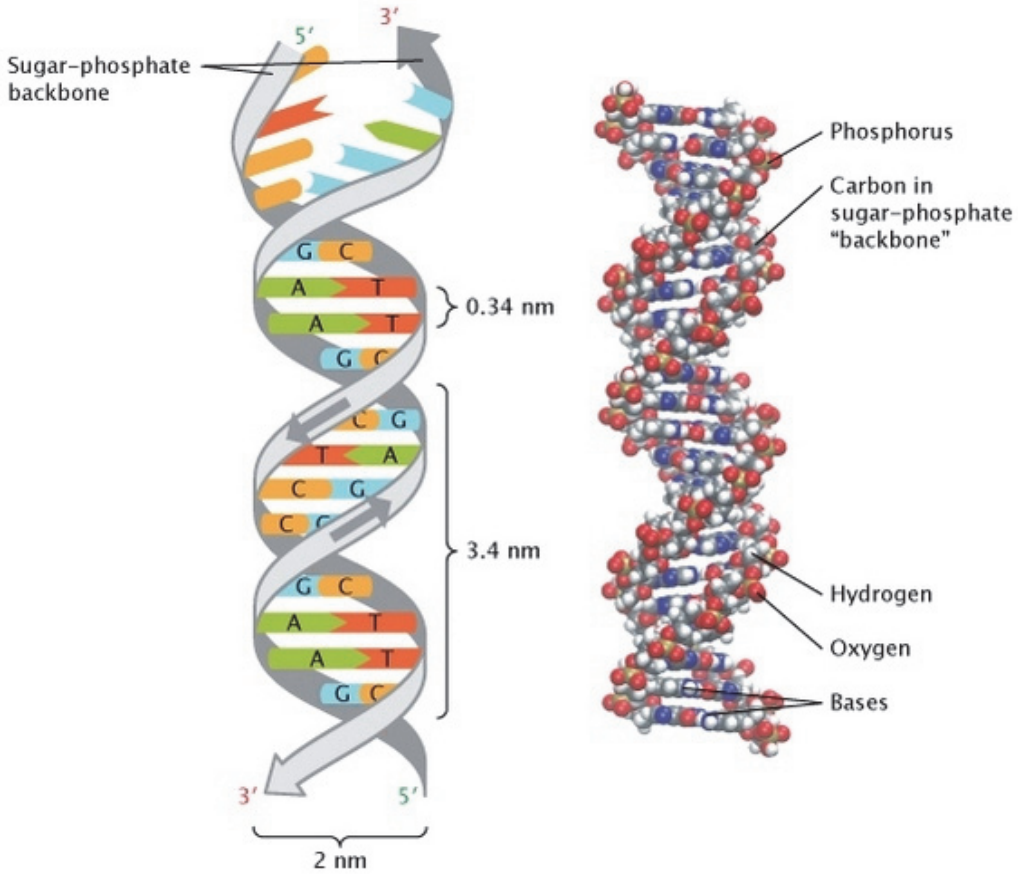

Figure 2. B-form DNA double helix. Illustration adopted from [23].

2.2 DNA Origami

The concept of scaffolded DNA origami was first proposed by Paul Rothermund in 2006, in which he used over 200 staple strands to hold a 7-kilobase long scaffold in place [4]. The shape was formed by linking several parallel helices together, which were connected by a periodic array of crossovers (Figure 3a).

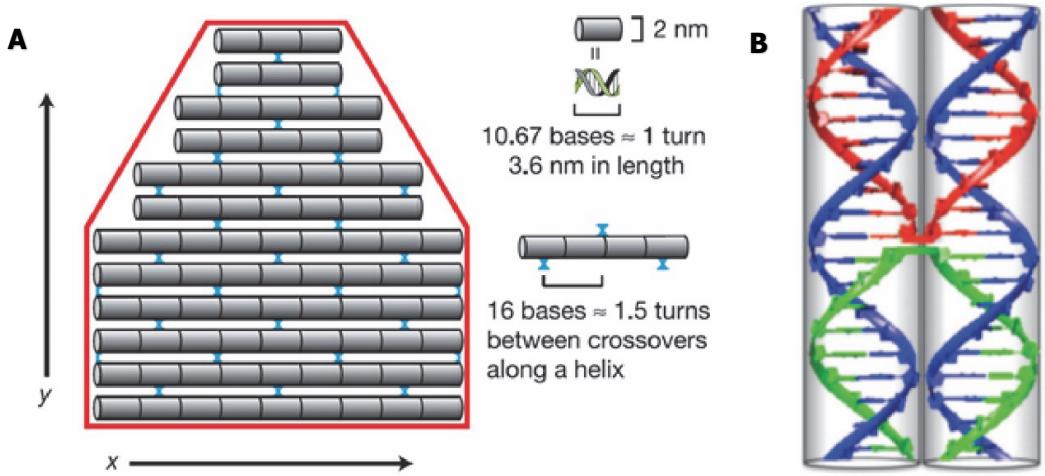

Figure 3. (A) Crossover scheme and helices packing in Paul Rothermund's paper (B) Backbone orientation of two adjacent helices with crossovers occur when two backbones come into contact. Illustration adopted from [25].

In the paper, the author explained crossover spacing rules, an important principle fundamental to subsequent developments in DNA origami.

By definition, a crossover is formed when one strand of a double helix crosses over to an adjacent helix, thereby connecting the two together. If these connections are placed where the backbones of the two helices in question come into contact, then no additional base is needed to traverse the space that would otherwise be present if two backbones are further apart (Figure 3b). Due to the periodic twist of helix, these contact points occur once every two full turns, corresponding to 21 base pairs (bps) for B-form double helix. In essence, these rules dictate that the distance between any two crossovers would depend on the angle formed between them (Figure 4b), and these also apply to structures where more than two helices are used.

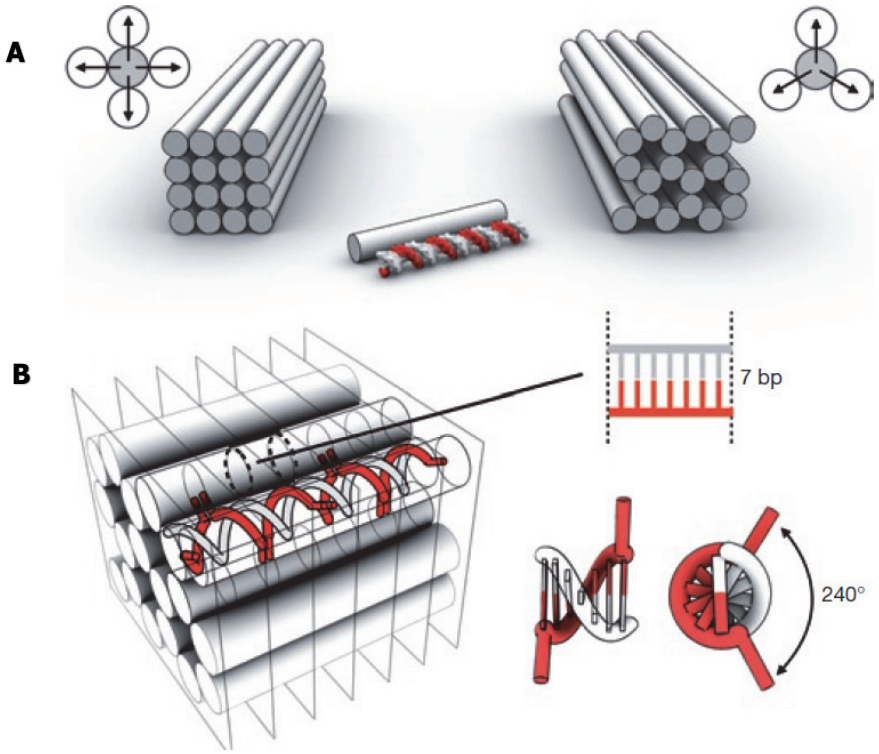

Figure 4. Helix packing and crossover-spacing rules for 3D DNA origami. (A) DNA origami objects designed with square lattice (left) and honeycomb lattice (right). (B) Crossover spacing for honeycomb lattice packing, with two adjacent crossovers spaced 7 bps apart, corresponding to a backbone rotation of 240°. Illustration adopted from [6].

Based on that rationale, a honeycomb- and square-lattice framework was developed where the distance between any two crossovers reflects their corresponding angle [16], [26]. For example, in a honeycomb lattice where the angle is 120° (Figure 4), crossovers can be located every 7 bps or two-thirds of a turn. For square lattice, the interval would be 8 bps.

From Table 1, one could see that while structures designed in a honeycomb lattice conforms to the natural B-form of DNA, square-lattice structures would experience underwinding, which would lead to a global right-handed twist [6]. One way to correct this inherent global twist is to remove some base pairs from every helix in a twisted structure so that the natural number of bps/turn is restored [6].

Table 1. Natural DNA double helix geometrical properties and as assumed in honeycomb and square lattice

	Natural B-form	Honeycomb lattice [26]	Square lattice [16]
Length per bp (nm)	0.34	0.34	0.34
Twist per bp	34.3°	34.3°	33.75°
Bps/turn	10.5	10.5	10.67

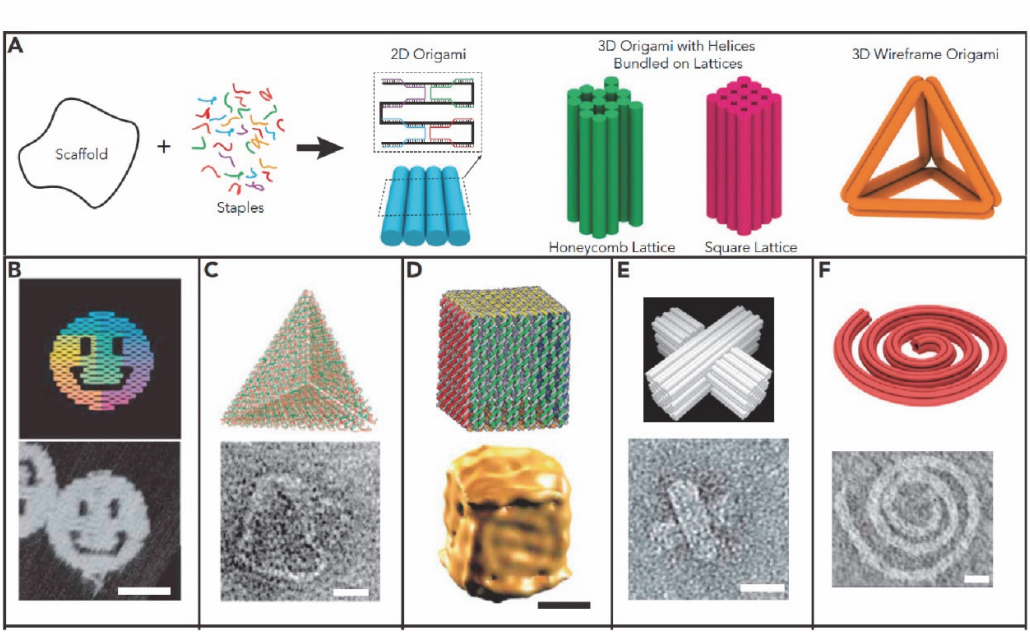

Figure 5. (A) DNA origami design strategies for 2D and 3D structures [3]. (B) DNA single-layer structure, a smiley face [4]. (C and D) Hollow structures of tetrahedron [27] and cube [28]. (E and F) Examples of more complicated 3D structures: a slotted cross [26] and a spiral-like object [8]. Scale bars: 50nm (B), 20 nm (C-F).

In parallel with the above development from 2D to 3D structures, software packages were also built to streamline the design process. First is the introduction of caDNAno [5], which provides a design framework for both honeycomb and square lattice structures. The advent of caDNAno greatly facilitates the design process as the program automatically suggest ‘crossable’ positions along each helix so that the crossover spacing rule is satisfied.

Besides, various prediction tools were also developed for DNA origami structures, e.g. [6], [29], [30]. These tools are particularly helpful in guiding the design of complex objects with curvature and twist [6]. Figure 5 summarizes the design strategies for DNA origami and provides some examples of 2D and 3D DNA origami structures.

2.3 Building curvatures in DNA origami

2.3.1 Terminology

Below are some terminologies used in describing design of DNA-origami-based curvatures, most of them were used previously in literature while others are adopted for the first time herein for brevity.

For a curved, multilayer DNA origami structure, *vertical direction* is perpendicular to the curving direction while *concentric direction* is parallel to it (Figure 6).

Degree of curvature is formally defined as the central angle to the ends of an arc. All designs implemented in this thesis have a 360 degree of curvature, yet the principles outlined herein can be extended to any degree of curvature, e.g. half circle.

Insertion and *deletion* of a single base as implemented in caDNAno will be referred to collectively as *modification*.

Length gradients mean the difference in number of bps between neighboring helices in the concentric direction, containing the information necessary to design a structure of a particular cross-section type, with a particular degree of curvature (Figure 11, Figure 12).

Number of bps/turn after modification is calculated by dividing helix length after modification to the original number of turns. Although it is unclear if this metric truly reflects the actual conformation of double helix after modification, it is a useful proxy for how much a design deviates from crossover spacing rules. It has been observed that extreme deviation (less than 6 bps/turn or more than 15 bps/turn) should be avoided [8].

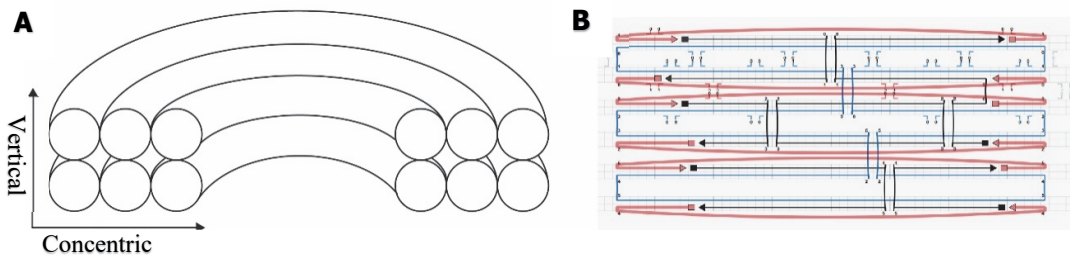

Figure 6. (A) Concentric and vertical direction, (B) Scaffold edges and bridging staples (red strands).

Regardless of scaffold routing patterns, there would always be an *edge* in a DNA double helix bundle (Figure 6b). For a curved bundle destined to be fully closed, the two edges would come into close proximity, and a set of short oligonucleotides can be used to connect them, called *bridging staples* (Figure 6b). The act of closing two edges with such staples is referred to as *bridging*.

Seed is a segment where the hybridization between two strands stretches uninterrupted by crossovers for at least 14 bps. These segments are hypothesized to facilitate folding by nucleating specific attachment to the scaffold [31].

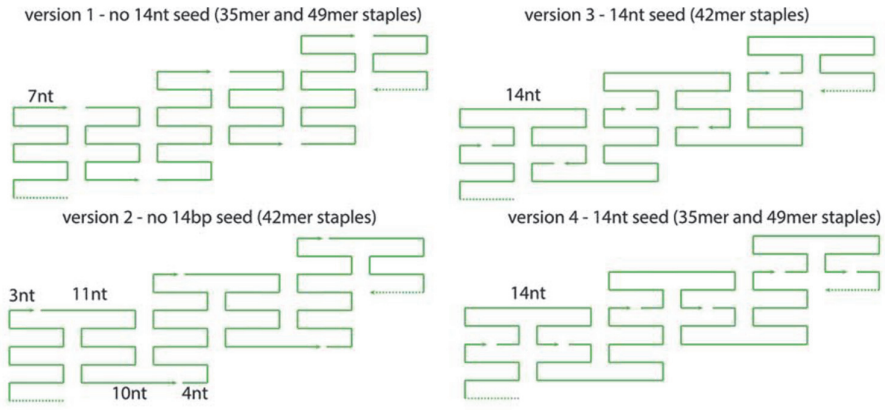

Figure 7. Four different designs with (right) or without seed (left) for each staple. Illustration adopted from [31].

On-lattice and *off-lattice* denote whether a design uses the lattice framework provide by caDNAno, hence *on*, or not. While the former option makes use of caDNAno ability

to keep track of suitable crossover positions, the latter provides more freedom in placing crossovers at user-defined locations. This freedom could be useful when a lot of modifications are used but time-consuming for a large, multilayer structures.

Two strategies have been proposed to design curvature using DNA origami, each based on either the on- or off-lattice framework above. These two will be explained separately in the next two sections.

2.3.2 Designing twist and curvature with on-lattice framework

The first strategy uses the on-lattice framework provided by caDNAno, creating twist and curvature by introducing targeted insertions and deletions of bp into DNA bundles, so that the interval between two adjacent crossovers no longer conforms to the crossover spacing rule outlined in Section 2.2 [8]. Consequently, there would be a global relaxation of the DNA helix bundle to compensate for this deviation and adopt the desired conformation (Figure 8).

In the case of twist, insertions or deletions are introduced uniformly in all helices present in a cross-section, causing underwinding/overwinding, which would consequently be compensated by the global relaxation of the structure into a right-handed/left-handed twist.

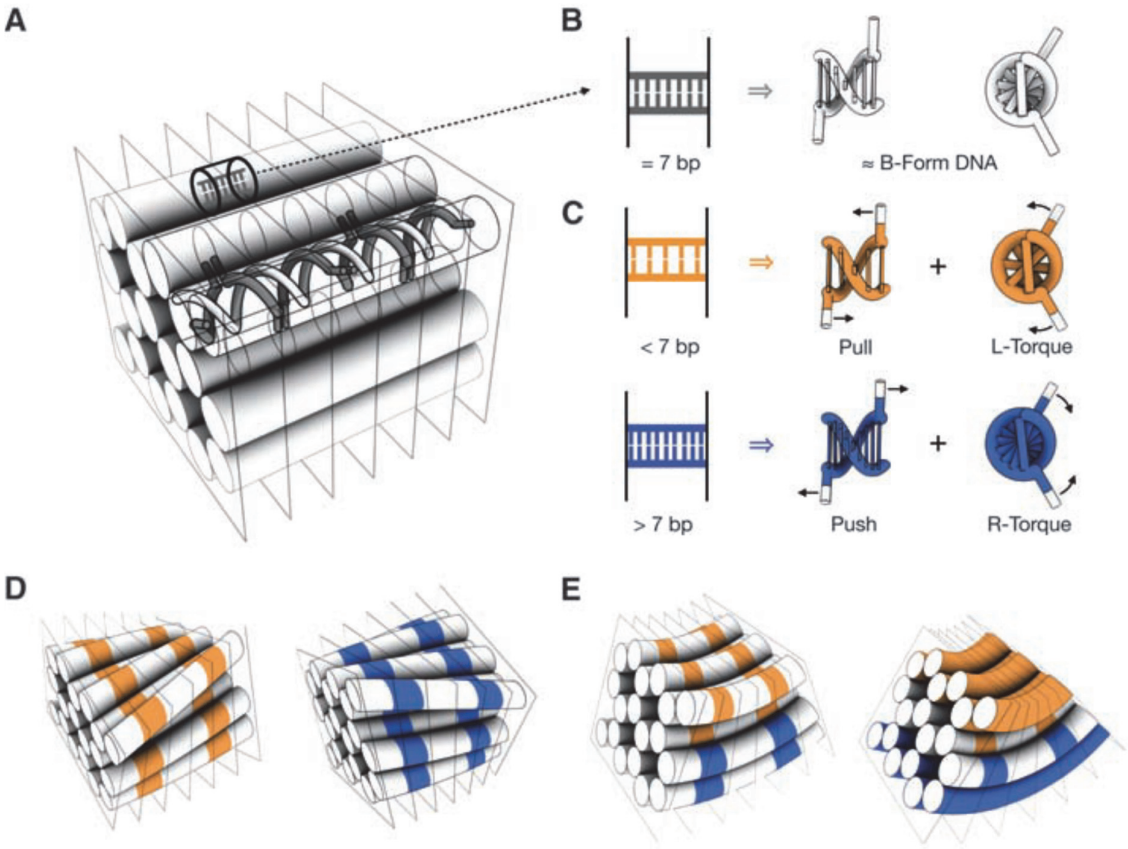

Figure 8. Design principles for twist and curvature in DNA bundles. (A) Double helices are packed into a honeycomb lattice, with crossovers spaced at 7-bp intervals along helical axis. (B) Array cell with default number of 7 bps, thus following the natural conformation of B-form DNA double helix and placing no stress on its neighbors. (C) Above, after deletion, 5 bps remains in the cell, which exerts a pull on its neighbors. Below, conversely, after insertions, array cell exerts a push on its neighbors. (D) (Left) Targeted deletions at orange cells result in global left-handed twisting; (right) targeted insertions in blue cells result in global right-handed twisting. (E) Targeted deletions and insertions are combined to produce global bending. Illustration adopted from [8].

For curvature, the cross section of a structure will be divided into various layers, and a decreasing gradation of number of bps/turn from the outer to the inner layer will be created by inserting and deleting several bps. Similar to the case of twist, when the number of bps/turn of a helix is abnormal, the structure tends to compensate for this

deviation by extending in the outer and compressing in the inner layers. These two opposing forces will be put to work in conjunction by a system of crossovers, connecting both ends of two adjacent helix segments to each other (Figure 9). The more crossovers there are, the more rigidity the system has [16]. Without these crossovers, each helix would just extent or contract independently, forming a collection of straight helices with uneven lengths.

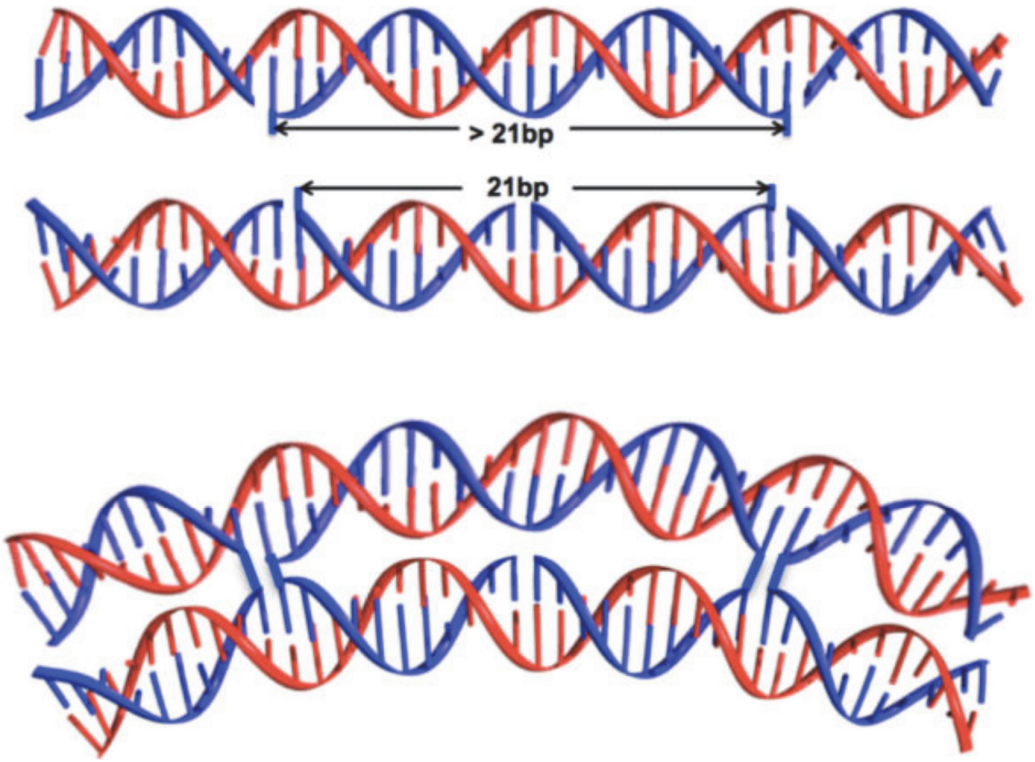

Figure 9. Two helix segments with different length before and after being connected by crossovers. [25]

The key here is to strike a balance between extension and compression, which can be achieved by ensuring that the average number of bps/turn throughout the structure conforms to the natural 10.5 bps/turn. That said, the number of bps/turn in the outer and inner layers would still deviate significantly from the natural parameter, leading to high degree of internal tension, thus hamper high-yield assembly and structure integrity [8].

The first limitation of this paper is the lack of well-defined guideline for designing a structure with particular degree of curvature. A toy model with various parameters

such as stretch, bending, and twist-stretch-coupling moduli of DNA was proposed to predict the degree of curvature, yet despite the several physical parameters involved, the model did not have robust predictive power, necessitating an iterative design and simulation process combining caDNAno and CanDo [8].

Additionally, since both curvature and twist formation using this approach relies on the global relaxation of the structure, a suboptimal design of curvature will be prone to a small amount of twist. This will be a challenge for designs of high precision, for example when a curvature need to be closed by bridging two ends.

The twisted curvature problem is further exacerbated in the case of square-lattice structures with their inherent twist and could be the reason currently there is no implementation of square-lattice curvature found in literature.

The above limitations are unwanted consequence of using on-lattice design framework in caDNAno, which inevitably violates of crossover spacing rules. The second approach below would address these shortcomings.

2.3.3 Off-lattice curvature

Another study on building complex curved DNA origami objects proposed a design strategy that gives a greater level of control to the geometry of the structure and also observes crossover spacing rule so that the natural number of bps/turn is preserved [9]. Accordingly, the steps to create a curved structure of arbitrary shape involve (1) calculating and implementing the length gradients between helices in adjacent concentric layers, given a particular cross-section, (2) determining the distance between neighboring crossovers so that they are evenly distributed throughout the structure and the natural state of DNA double helix is preserved as closely as possible. The following part will explain in details how these two steps are put to work in a planar concentric rings system, i.e. all rings lie in the same surface, both for illustrative purpose and its relevance to the design of a square-lattice curvature.

First, to calculate length gradients, the overall geometry of the structure has to be considered. In a concentric rings system (Figure 6a), the relationship between length difference (ΔC) and diameter difference (Δd) of two rings would be given by

$$\Delta C = \pi \Delta d \qquad \text{(Equation 2.1)}$$

For two adjacent helices assumed to be strictly contiguous, i.e. interhelical distance is zero, Δd will simply be the diameter of DNA double helix (Figure 6a). The interhelical distance would be compensated for by using *effective diameter,* which was measured by TEM for DNA origami objects to be about 2.3-2.6 nm [32], rather than the natural diameter of 2.0 nm.

The above value of length difference, calculated to be 15.7 nm, would then be converted to the equivalent number of bases which is 48.5, assuming natural, B-form twist density of DNA (10.5 bps/3.4 nm). As only integer values are acceptable and those with natural symmetry are preferred (so that crossovers can be evenly distributed), that value is rounded to 48 or 50 bps. In short, each ring in the concentric rings system would differ by 48 or 50 bps from its immediate, concentric neighbors while those in the same vertical layer have identical length. Following this calculation, the rings system is expected to be planar without experiencing any strain caused by a design pattern that deviates significantly from the crossover spacing rules.

If the first step shows a quantitative way of determining how much length difference is required among concentric layers to preserve the natural state of DNA B-form helix, the second step ensures that the distance between any two crossovers in the system conforms to the crossover spacing rules, with the same purpose of avoiding unnecessary strain.

After the length of each ring in the system is determined, the next step would be placing crossovers evenly throughout the structure to ensure symmetry and rigidity. Also, to ensure natural conformation of B-DNA, intervals between crossovers of the same type have to be multiples of 10.5. For simplicity, 10 can be used instead of 10.5 because it is an integer and makes it easier to satisfy the 50 bps length difference requirement as shown in Figure 10.

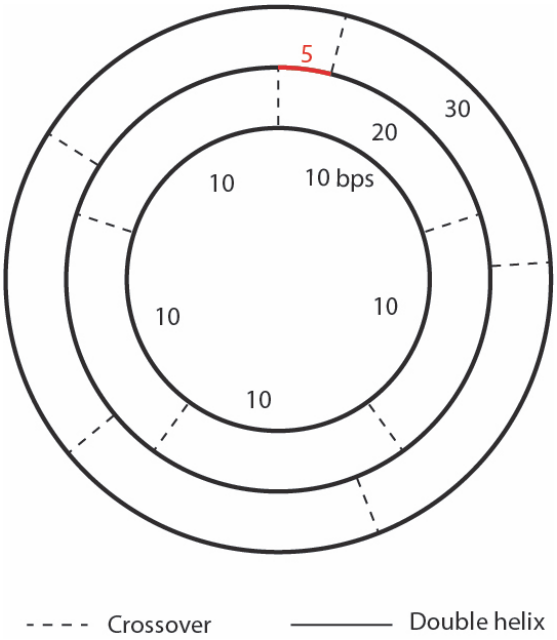

Figure 10. Example of the crossover layout for a planar 3-concentric-ring system as described above. Additionally, since crossovers from 1st to 2nd and 2nd to 3rd form a 180° angle, the distance between them should be an odd number of half turns [4]. Illustration simplified based on [9].

Although this approach provides a solid framework to build curvature of complex shape, it has not been validated for a 3D structure, and another limitation is the lack of an automated tool to keep track of the crossover system and export sequence similar to caDNAno.

This section sheds lights on the development of DNA origami structures with a specific focus on twist and curvature using this technique. Although designing such complex objects has been achieved satisfactorily for several years, there are still some area for validation. Specifically, it would be desirable to (1) validate the off-lattice (or geometry-based) method in building 3D curvature, (2) build a square-lattice curvature. However, for the lack of automated framework to aid the design process, the designs of curvatures in this thesis will only follow step 1 of the geometry-based approach, i.e. the length of each layer will be determined by its relative position to immediate neighbors. These geometry-based calculations will then be implemented by caDNAno

using its insert/delete feature, and thus the crossover spacing rules will not receive due consideration and be a subject for future exploration.

3 Materials and Methods

3.1 Designing principles for DNA origami curvatures

- Length gradients are calculated based on the cross-section of a particular structure, taking into account the geometry of natural B-form DNA double helix. Other physical parameters, such as axial stiffness, bending stiffness, torsional stiffness, nick stiffness factor, are ignored.
- Length gradients will be implemented using insert/delete feature of caDNAno. Modifications are spread out evenly throughout the structure to ensure symmetry [8].

3.1.1 Length gradients calculation for each type of cross-section

The length gradients are determined using simple geometry. For honeycomb lattice, every three neighboring helices form a triangle ABC as in Figure 11, with $AB = D_{helix}$. Thus, $d_1 = \frac{1}{2}BC = AB * sin60 = D_{helix}\frac{\sqrt{3}}{2}$. d_2 and d_3 are simply the effective radius and diameter of helix, respectively.
With these values, Equation 2.1 is used to calculate length gradients in nm and the result subsequently converted to equivalent number of bps. The computed values for each D_{helix} value are summarized in Table 2.

Table 2. Length gradients calculated with different D_{helix} values

Distance	With natural D_{helix}, 2 nm	With effective D_{helix}, 2.5 nm
d_1	10.9 nm (33.5 bps)	13.6 nm (42 bps)
d_2	6.3 nm (19.5 bps)	7.85 nm (24 bps)
d_3	12.6 nm (39 bps)	15.7 nm (48.5 bps)

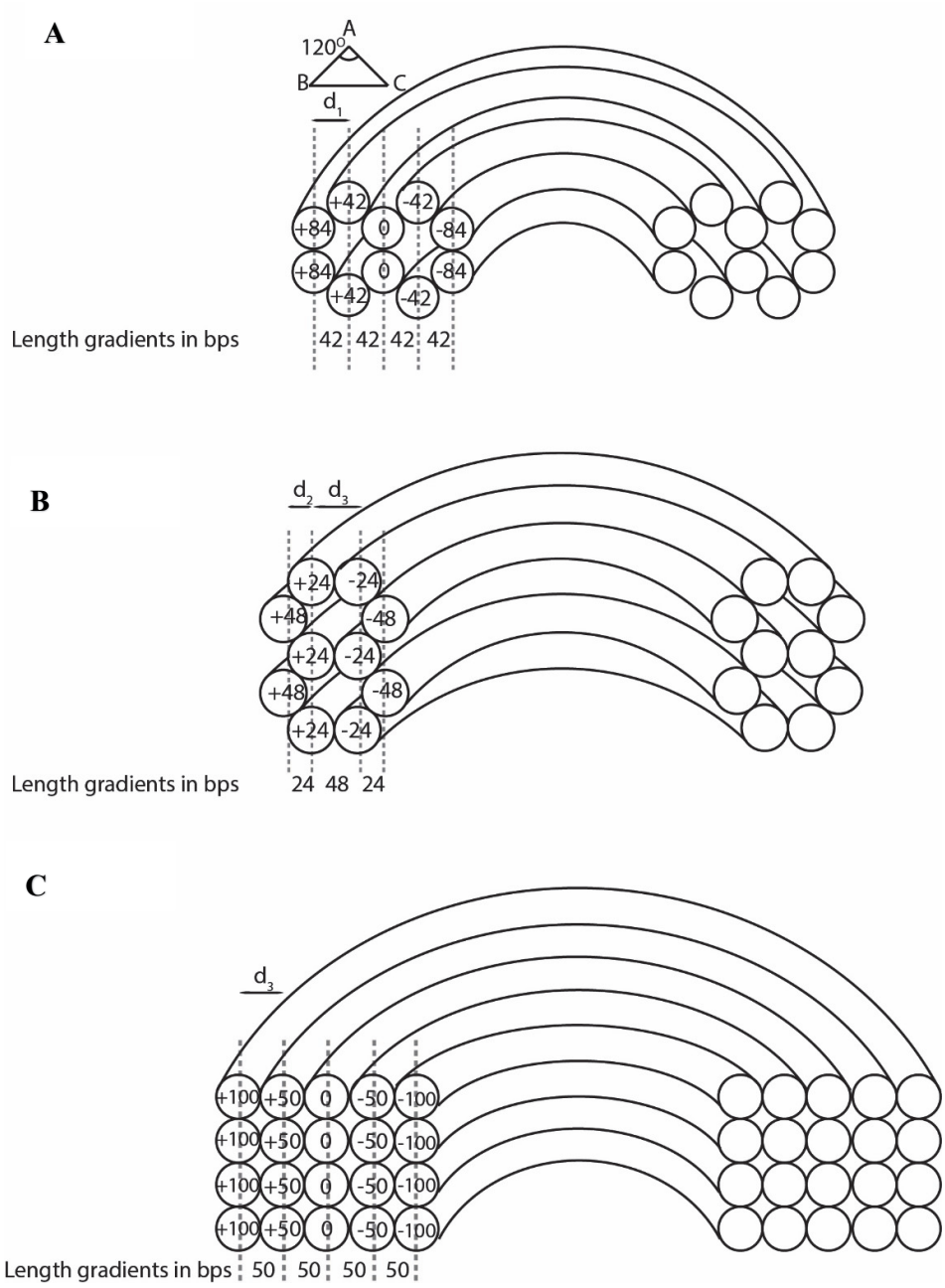

Figure 11. Three types of cross-section and corresponding length gradients (for D_{helix}=2.5 nm) to create fully closed structure (A, B are derived from honeycomb lattice and C from square lattice, only haft of the fully circular structures are shown). The number in each helix represents its number of modifications with positive sign for insertions and negative for deletions. These numbers can vary as long as the length gradients remain constant.

The above calculations are for fully closed curvature. For open structures with θ degree of curvature, their length gradients x can be approximated from the corresponding value y of closed structure with the formula:

$$x = y * \frac{\theta}{360} \qquad \text{(Equation 3.1)}$$

For example, for half ring (with 180^o degree of curvature) with cross-section type *a*, the length gradients would all be 21 bps.

3.1.2 Twist correction

Inherent twist in square-lattice origami structures can be rectified by deleting 1 per 64 bases along the helical direction of a structure [33]. Alternatively, since it has been suggested that resistance to torsion is a function of cross-sectional shape [8], [32], a cross-section with high torsional resistance, e.g. having multiple layers, will also minimize global twisting.

Thus, for the square-lattice ring, a rigid cross-section was chosen, and additional modifications were used to eliminate residual twist.

3.2 Structure predictions

Computer-aided engineering for DNA origami (CanDo) [6], [34] and another modeling tool [30] (henceforth referred to as AKSI) were used to guide the designing process.

For CanDo, length per helical rise was set at 0.34 nm as default and only effective helix diameter (default is 2.25 nm) was adjusted to 2.5 nm. Physical parameters such as stretch modulus, bend modulus, twist modulus were left as default.

For structure with high density of modification, CanDo did not work and AKSI was used. All simulations with this program were run with default settings.

Designs used for simulation are simplified to speed up iterations and circumvent many limitations of each simulation software in the following ways:

- Crossovers are automatically generated using caDNAno. Effect of crossover positions is assumed to be minimal.

- Bridging of staples are omitted, otherwise simulations crash or give illogical results. Thus, all simulations result in open arcs with varying degree of curvature, rather than fully closed rings.

- AKSI has an input size limits, and thus for structures exceeding 7000 bps, only three quarters of the original designs are used structure prediction.

3.3 Experimental validation

3.3.1 Preparation of DNA origami

3.3.1.1 DNA origami assembly

Each structure was assembled from a one-pot reaction mixture containing: scaffold strands of 7249 or 8064 bases (p7249 and p8064 respectively, TiliBit Nanosystem), [35], corresponding staples (Thermo Fischer Scientific), TE buffer, magnesium chloride, and distilled water.

A sample mixture with 5 nM of scaffold, 1:5 scaffold to staple ratio, and 20 mM $MgCl_2$ is presented in Table 3.

Table 3. Example assembly mixture for DNA origami structures

Reagent	Final concentration	Volume (µL)
10X TE buffer	1 X	5
100 nM scaffold	5 nM	2.5
500 nM staples	50 nM	5
100 mM $MgCl_2$	20 mM	10
100 mM NaCl	5 mM	2.5
Distilled Water	Fill to 50 µL	25

Table 4. Thermal annealing temperatures and times

Temperature, °C	Time, minutes
80	15
79, 78, …, 72, 71	1
70, 69, 68	5
67, 66, 65, 64, 63	10
62	15
61	20
60	30
59, 58, …, 39, 38	60
37, 36	45
35	30
34	20
33, 32	10
31, 30, …, 26, 25	5
24, 23, 22, 21	2
20	Hold

3.3.1.2 DNA origami particles purification

After assembly, polyethylene glycol (PEG) purification method [36] was used to remove excess staples and obtain the whole population of folded species. Assembly mixture and precipitation buffer (18% PEG-8000 (w/v), 1X TE buffer, 500 mM NaCl and 12.5 mM $MgCl_2$) were mixed with 1:1 volume ratio and then centrifuged for 30 mins at 20 000 g. Due to the depletion of high-molecular-weight species when a crowding agent, e.g. PEG, is added to a solution, DNA origami particles will precipitate into pellet form at the bottom of the centrifuged tube [37]. After supernatant has been carefully removed, the pellet is resuspended in 1X TE and 15 mM $MgCl_2$. The whole procedure is repeated 1 or 2 more times before the final pellet is left to

equilibrate overnight in the same resuspension solution or any other solution conducive to DNA origami stability [36]. The final solution will contain any high-molecular-weight particles including aggregation, various states of oligomerization and monomers.

For a more selective separation, e.g. when only a single species is needed, agarose gel electrophoresis was used, which separates particles based on their electrophoretic mobility [36]. The assembly mixture is loaded into 1% agarose gel already submerged in running buffer (0.5X TBE and 12 mM $MgCl_2$). The gel is then run for 3h at 80V in an ice-bath to prevent melting. After visualization under UV-light, the desired band is cut and extracted for later experiment.

3.3.1.3 Assembly condition screening

For multilayer structure, cationic strength of the folding solution is vital in achieving high assembly yield [3]. Thus, screening of optimal magnesium concentration for folding process of each structure was carried out as described elsewhere [26], [36].

Three criteria to determine optimal folding condition include:

- High intensity of desired band relative to other byproducts. For a monomeric DNA origami structure, the expected particles reside in the quickest-running band excluding staples band [26].
- Properly folded particles, due to their structural homogeneity, often constitue a clear, defined band whereas a smear often indicates a mixture of poorly folded particles with various defects and thus slightly different mobility [26].
- Samples will be extracted from the chosen band and structure integrity confirmed using negatively stained transmission electron microscopy.

3.3.2 Structure analysis

3.3.2.1 Negatively stained transmission electron microscopy

Purified samples are absorbed for 5 min onto discharged carbon-coated copper grids, stained for 40s with 2% uranyl formate, 25 mM NaOH, and visualized at 10 000x - 68 000x magnification with FEI Tecnai 12 Bio-Twin operating at 120 kV.

3.3.2.2 Yield estimation

- Based on gel intensity: Relative yield of an origami species is calculated as reported elsewhere [5]. The background-subtracted integrated intensity value of the band corresponding to the species of interest is divided by the total background-subtracted integrated intensity of all species, including smear. Gel images are analyzed by ImageJ.
- Counting on TEM images: All fully visible particles in TEM images are chosen for further counting. Intact particles are defined as well-folded ones with no visible discontinuity as compared to broken ones.

3.3.2.3 Diameter and degree of curvature estimation

Intact particles of each species were manually picked to measure diameters and degree of curvature with the aid of ImageJ.

4 Results and discussion

4.1 Design and simulation of three rings

To validate the design principles laid out in section 3.1, three fully closed curvatures (hence, rings) representing three types of cross-sections were designed. Two, V Ring and K Ring, conform to geometry-based calculations while the other, A Ring, is a replicate from literature for comparison (Figure 12). Design details for each are elaborated below and caDNAno designs can be found in appendix.

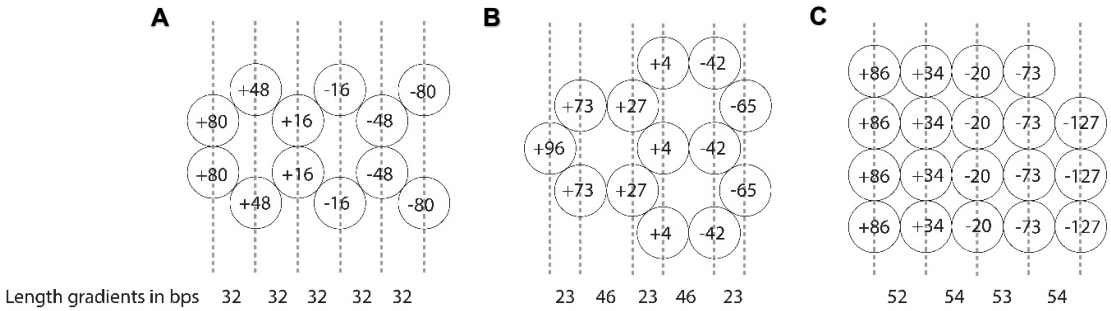

Figure 12. Cross sections and modification gradients for three designs: (A) A Ring, (B) K Ring, and (C) V Ring. The number in each helix represents the number of modifications in each helix.

4.1.1 Rings with honeycomb-lattice cross-sections

A Ring corresponds to the first type of cross-section derived from honeycomb lattice (Figure 12a). This design is intended to be a ring in its original paper [10] and is replicated here with number of modifications and crossover pattern kept identical to the original design.

Table 5. Helix lengths before and after modification for A ring

Concentric layer	Helix length before modification (bps)	Helix length after modification (bps)	Number of bps/turn after modification
1st	672	592	9.25
2nd	672	624	9.75
3rd	672	656	10.25
4th	672	688	10.75
5th	672	720	11.25
6th	672	752	11.75

The second type of cross-section from honeycomb lattice is tested with K ring, which was designed from scratch using the proposed principles. Compared to A ring, this design has more vertical layers, which presumably increase the rigidity of the structure and thus its ability to enforce curvature.

Table 5 and Table 6 summarize essential features of these two curvatures.

Table 6. Helix lengths before and after modification for K ring

Concentric layer	Helix length before modification (bps)	Helix length after modification (bps)	Number of bps/turn after modification
1st	546	481	9.25
2nd	546	504	9.69
3rd	546	550	10.58
4th	546	573	11.01
5th	546	619	11.90
6th	546	642	12.35

Figure 13 shows CANDO simulation results for A and K ring, indicating a slight twist and an open conformation for A ring. Using Equation 3.1, the degree of curvature for this design was estimated to be 274°, agreeing well with the model. The simulations also shows that even with similar degree of modification, K ring was less prone to global twist than A ring, confirming the hypothesis that cross-sectional rigidity played a role in reducing twist.

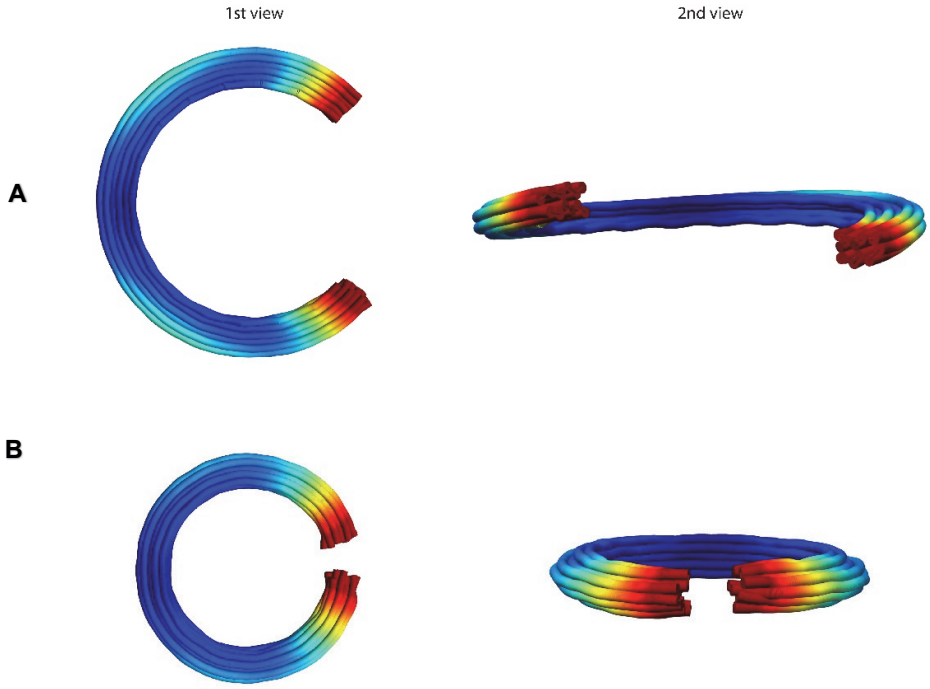

Figure 13. CanDo simulations for two honeycomb-lattice rings. (A) A ring, degree of curvature of the model is 277°. (B) K ring. All bridging staples are omitted, illustrated to scale.

4.1.2 Ring with square-lattice cross-section

This design, V ring, also followed the principles outlined in section 3.1. Its cross-section is illustrated in Figure 12c, one missing helix in the innermost (1st) concentric layer is due to limitation in scaffold length. The actual length gradients differs by 4

bps from the optimal value calculated in section 3.1.1. This, while avoidable, simplifies the designing process in caDNAno and is assumed inconsequential.

Table 7. Helix lengths before and after modification for V ring

Concentric layer	Helix length before modification (bps)	Helix length after modification (bps)	Number of bps/turn after modification
1st	427	300	7.50
2nd	427	354	8.85
3rd	427	407	10.18
4th	427	461	11.53
5th	427	513	12.83

In order to study the effect of twist in square-lattice curvatures, two more designs with different cross-sections and helix lengths were also used for simulation in AKSI (Figure 14). The modelling effort with these three designs, while did not lead to any concrete insights as to how a square-lattice-based curvature might twist, did provide some evidence for the role of cross-sectional rigidity in twist elimination, as is obvious when design *a* is compared to design *b* and *c* (V ring) in Figure 14.

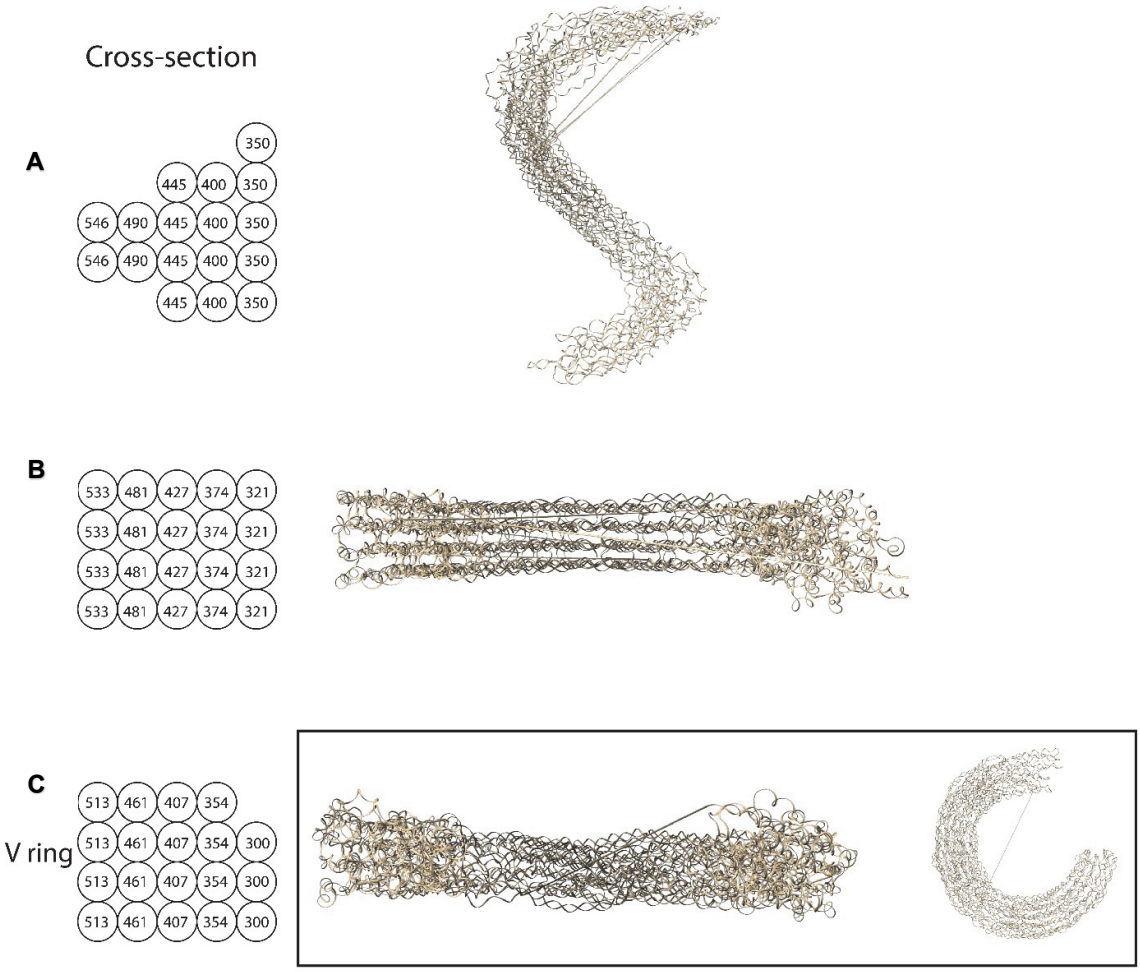

Figure 14. AKSI simulations for 3 square-lattice-based curvatures. Number in each helix denotes its length in bps. Note that only three-quarters of designs B and C were used for simulation.

4.2 Structure assembly and analysis

4.2.1 Assembly condition screening and yield

Optimal magnesium condition screening for A ring and K ring are shown in Figure 15. Using criteria outlined in section 3.3.1.3, 10 mM of $MgCl_2$ was the optimal magnesium

concentration for assembly of both A Ring and K Ring. The desired shape and dimension of each structure were also confirmed by using TEM (Figure 17).

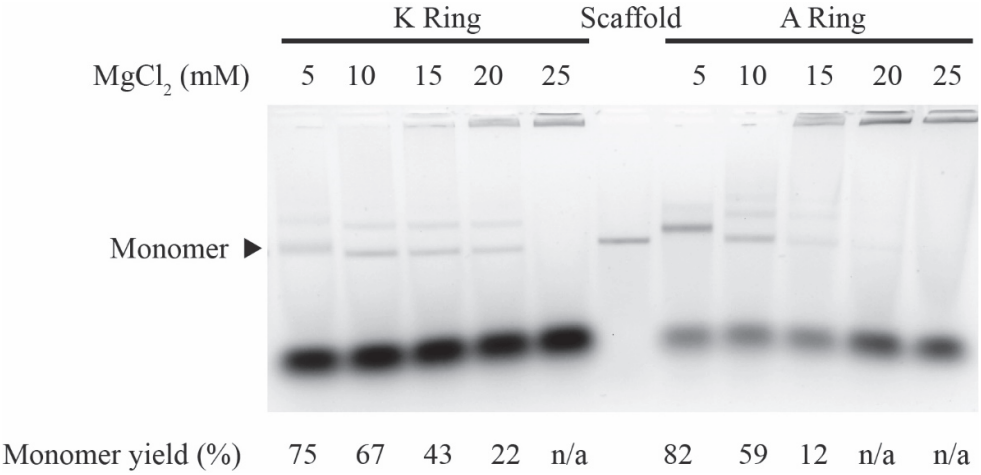

Figure 15. Magnesium screening for A ring and K ring.

For V Ring, gel analysis showed that assembly at 5 mM of $MgCl_2$ gives the most intense monomer band, while higher salt concentration results in significant aggregation. However, upon closer inspection under TEM, particles assembled in increasingly higher cationic strengths have more defined structures, and better resemble the designed shape. Thus, 20 mM of $MgCl_2$ was chosen as the optimal folding condition for both structural integrity and yield (Figure 16).

The fact that a square-lattice-based structure could only be assembled at a higher salt concentration compared to honeycomb-lattice ones could be explained by the higher density of helix packing [38].

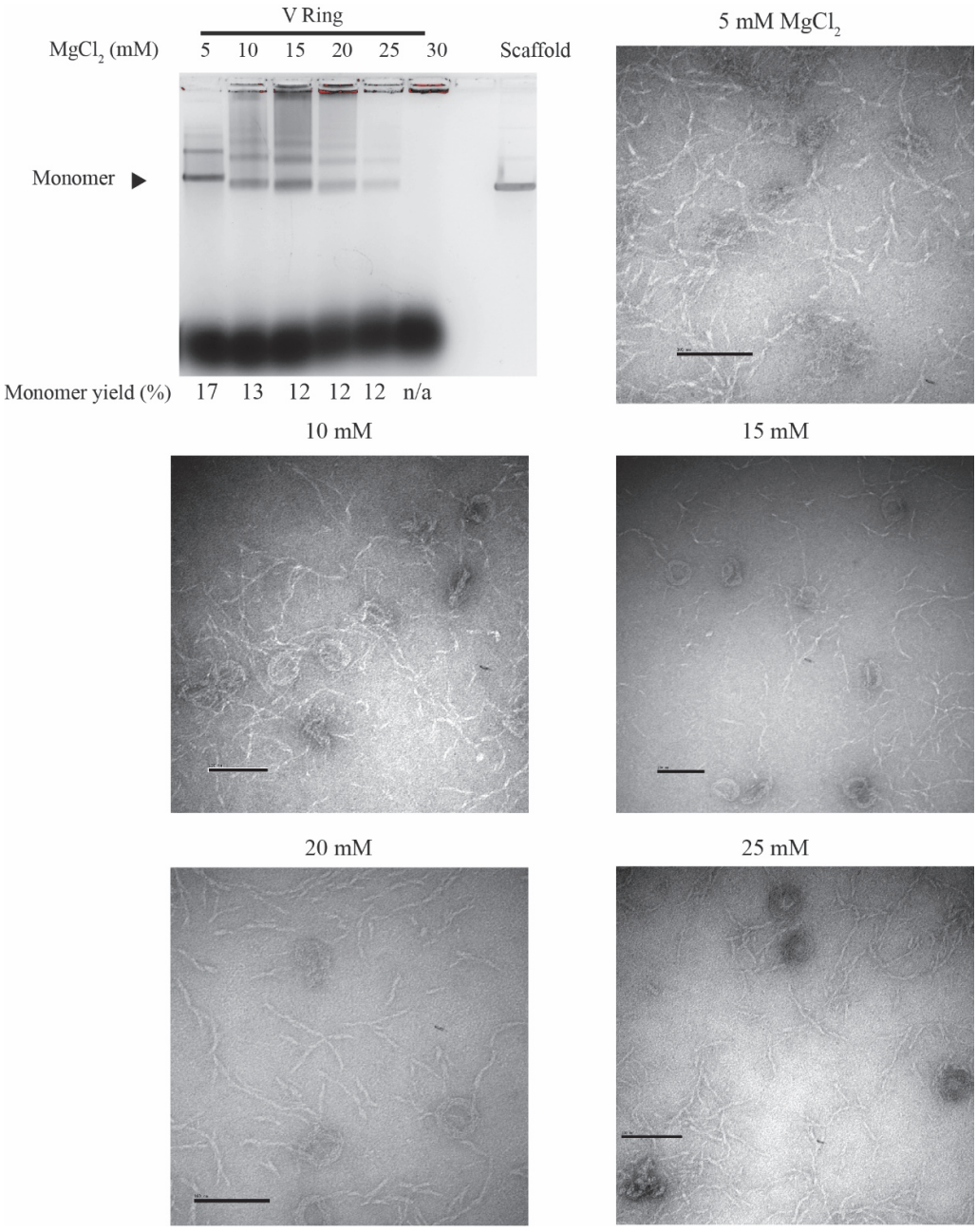

Figure 16. Magnesium screening for V ring and TEM images for each monomer bands. Scale bar 100 nm.

4.2.2 Exemplary structure

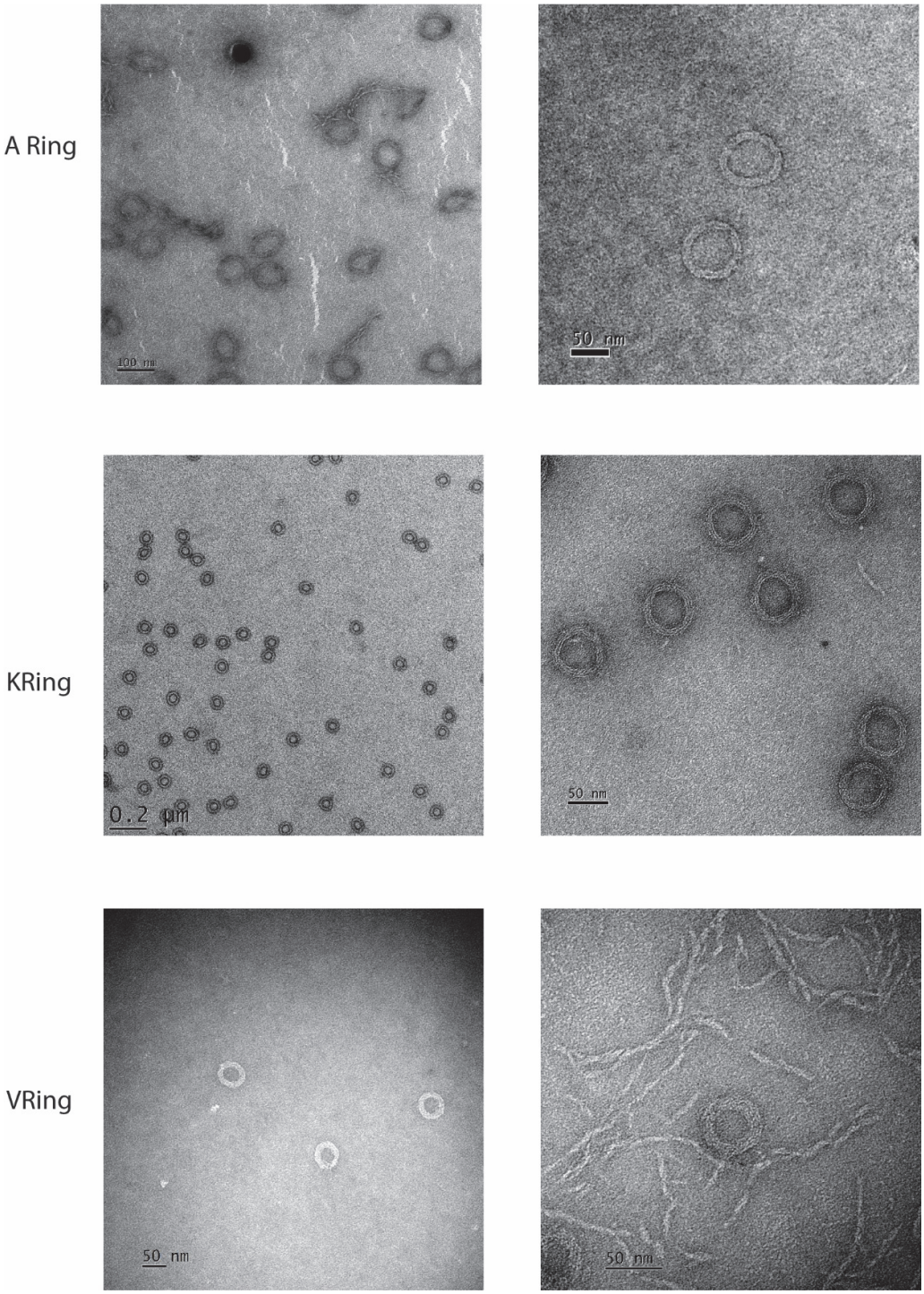

Figure 17. Exemplary images of all structures

Table 8. Designed and observed diameters of 3 rings. n is number of particles.

Structure	Designed diameter (nm)	Observed diameter (nm)
A Ring	79.2	79.6 ± 2.5 (n = 27)
V Ring	52.9	54.2 ± 1.2 (n = 15)
K Ring	66.2	65.2 ± 1.1 (n = 50)

4.2.3 Aggregation and oligomerization

Aggregation and oligomerization were significant problems preventing high yield assembly of curvature, the extent of which showed a positive correlation with salt concentration as can be observed in Figure 15 and Figure 16. Accordingly, V ring had the highest degree of aggregation, already visible in gel at 10 mM of $MgCl_2$, while A ring and K ring only started to aggregate at 20 mM. Figure 18 shows aggregation of each structure observed under TEM.

A possible explanation for this is the violation of crossover spacing rules that could prevent the intended crossover to take place. This will give rise to half-folded structure with several single stranded 'tentacles' that can reach out to hybridize with other half-folded scaffolds, resulting in a mesh-like aggregate. Indeed, V ring was the structure with the most extreme number of bps/turn after modification relative to the other two structures (Table 5, Table 6, Table 7). Moreover, the average number of bps/turn throughout the structure in V ring also deviates from the natural 10.5.

Another explanation for high degree of aggregation concerns the number of staples with more than one seed position. Among the three structures, there is a correlation between the severity of aggregation and proportion of staples with two seeds. Specifically, if a hybridization length of 12 is chosen as a cut-off value above which a position is considered *seed*, up to 80% of V Ring staples have two such positions, while the corresponding measures for A ring and K Ring are close to 0. This issue is avoidable and not an inherent trade-off of the design principles outlined in section 3.1. For a deeper understanding of why many two-seed staples lead to aggregation, the following hypothesis can be considered. Due to the high ratio of staples to scaffold (5 to 1 or higher), there is a possibility that two or more staples of the same type, i.e. of

identical sequence, can bind to one scaffold molecule, which will prevent proper folding. However, these undesirable hybridizations can be reversible if the binding energy is not too high, allowing for one staple strand to gradually replace others of its kind, via toehold-strand displacement, and eventually monopolize a particular scaffold. In order for that to happen, a staple can have only one seed, high-energy-binding, position to the scaffold, no matter how many scaffold helices it traverses. Examples for designs that conform to this rule can be found in in Figure 7.

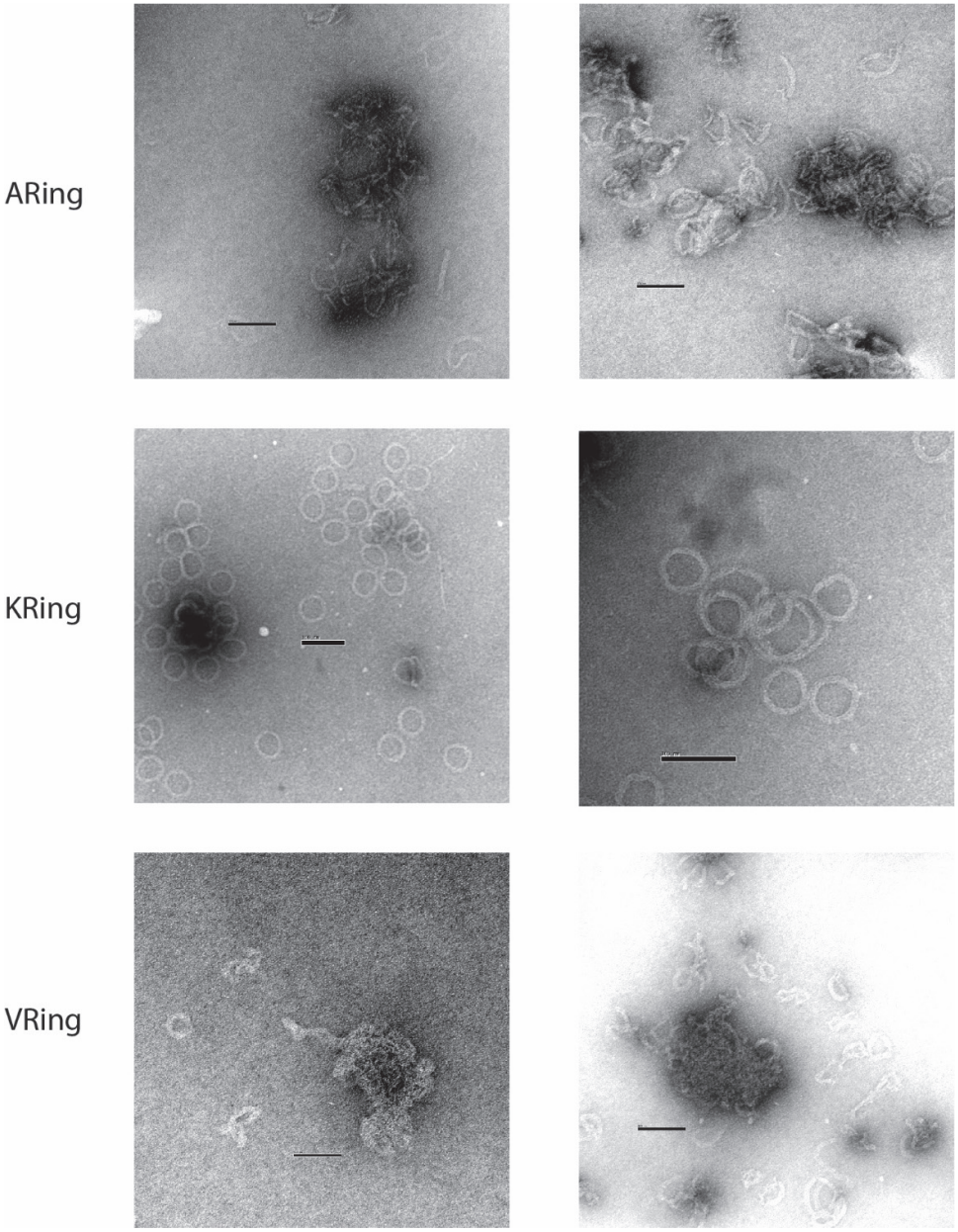

Figure 18. TEM images of aggregation in three structures. Scale bar 100 nm.

4.2.4 Other common types of defects

Besides aggregation, suboptimal designs will results in various structure abnormalities, the most noteworthy of which are shown in Figure 19.

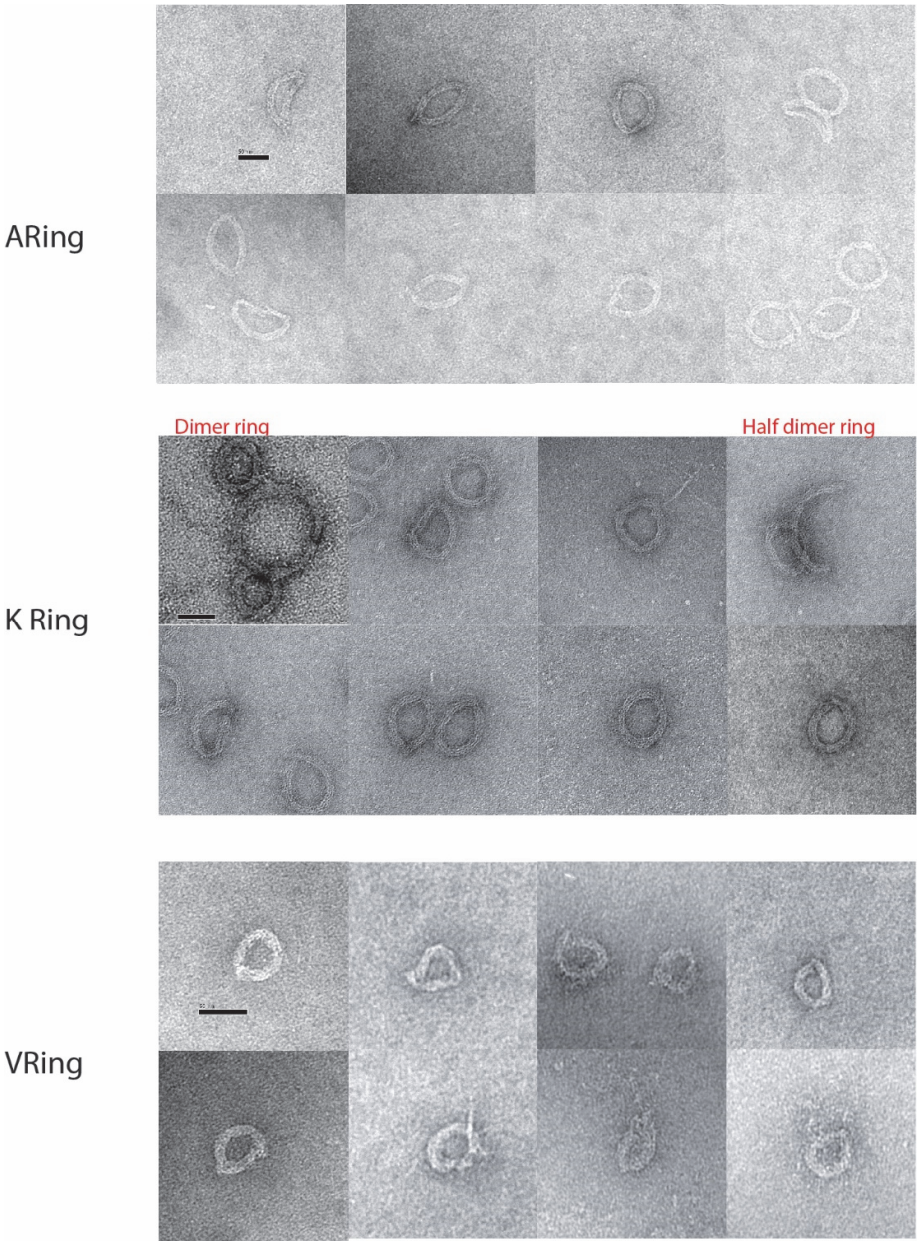

Figure 19. Common defects in three rings. Scale bar 50 nm.

4.2.4.1 Break in structures

For all three rings, a common problem besides aggregation is the occurrence of various breaks along helix bundles. Judging from TEM images, the extent of this problem varies for three rings, with V ring affected the most.

Figure 20 shows a comparison in terms of break prevalence in two honeycomb-lattice-based rings. V ring was excluded from this analysis due to the vanishingly small number of exemplary structure observed under TEM.

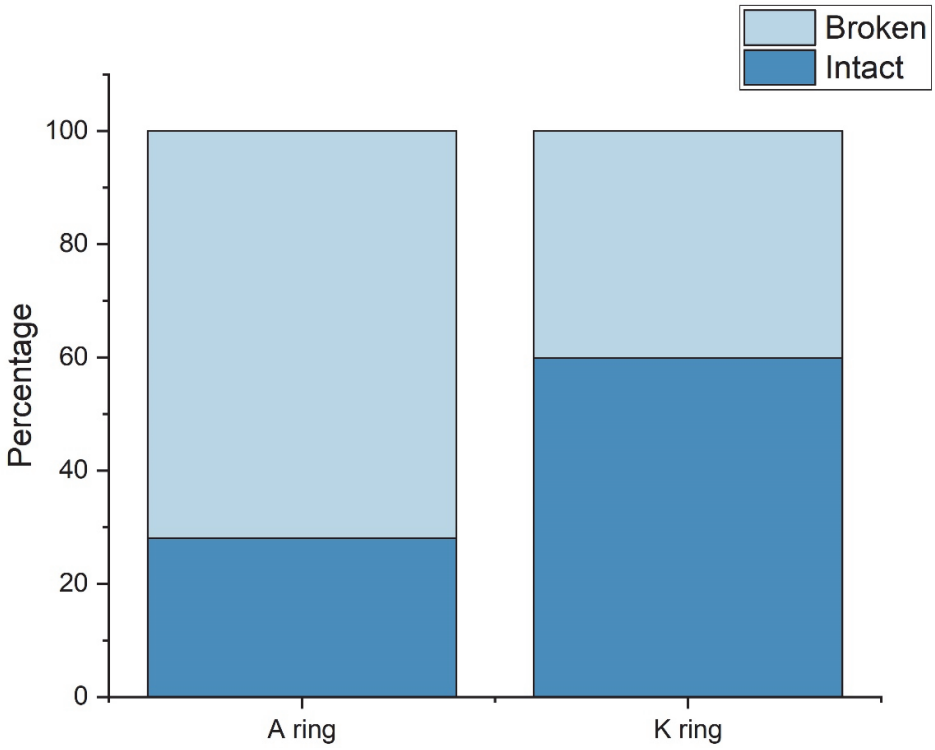

Figure 20. Percentage of intact particles in A ring and K ring present in monomer band extracted after gel electrophoresis (Figure 15). 230 random particles of each were examined. A particle is considered intact when it is fully circular and there is no visible break.

To better observe the degree of curvature in A ring, its subset of bridging staples were omitted from the assembly mixture so that there would be no forced bridging between the two edges, and thus the structure would be free to follow its most natural

conformation. The resultant structure is referred to as *open A ring*, shown in Figure 21.

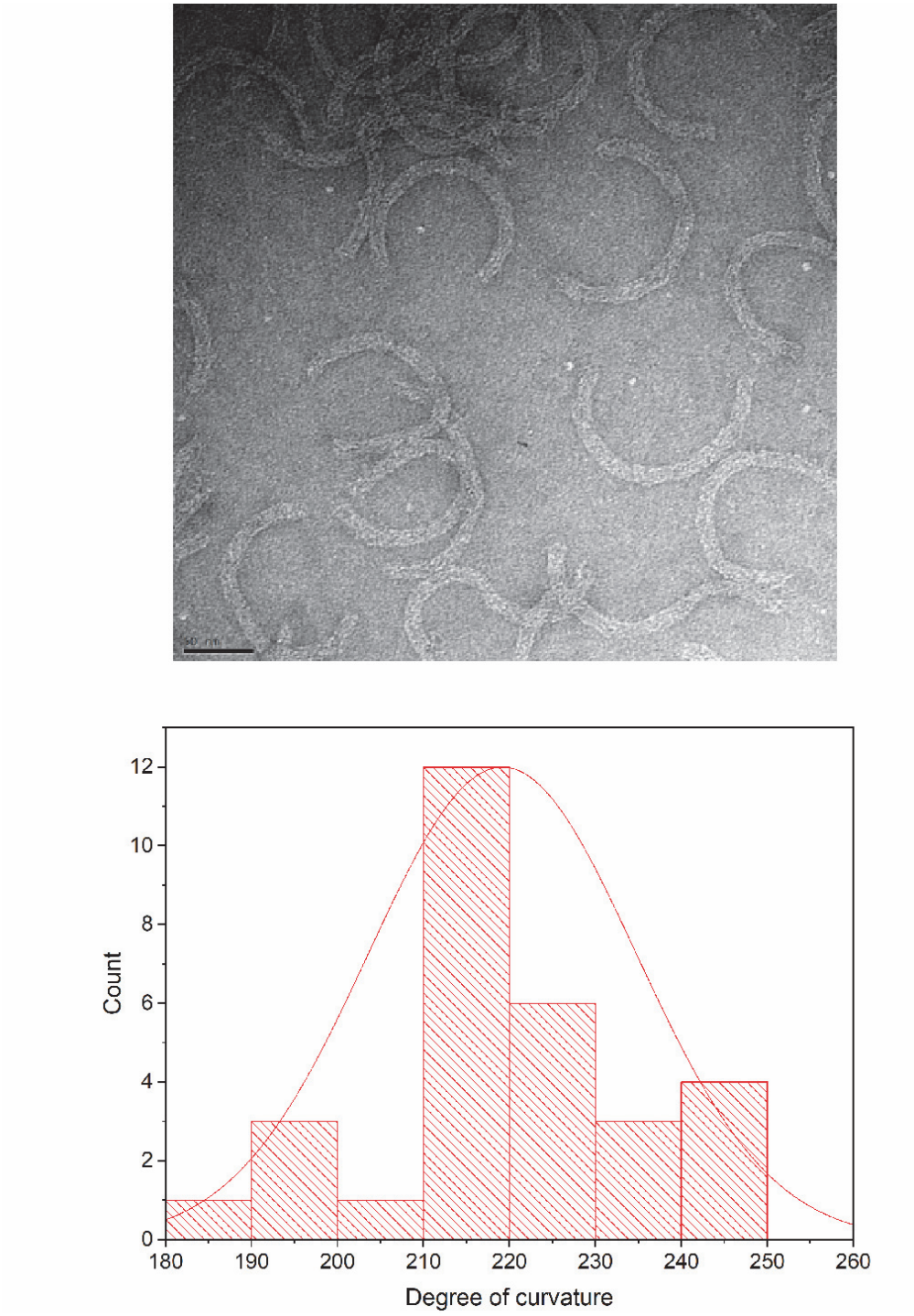

Figure 21. Open A ring and its angle distribution measured from TEM images. Average angle $219^{o} \pm 15.2$. Scale bar 50 nm.

Based on Equation 3.1 the theoretical degree of curvature for open A ring would be 274^o, which is in agreement with the angle observed from CanDo simulation (277°, Figure 13). Length reduction from the omission of bridging staples is assumed minimal.

The low value of observed angle in open A ring helps explain the high prevalence of breaks in its corresponding closed conformation. Specifically, if two ends of the structure do not come into proximity, a forced bridging might still close their gap, at the expense of structural continuity, i.e. the breaks observed in a large population of A ring.

Secondly, the significant deviation of the observed angle from both estimates shows that the geometry-based calculation in section 3.1.1 does not work well for structures of low cross-sectional rigidity like A ring. Presumably, the low number of vertical layers, or, thickness of structure, results in insufficient rigidity required to enforce the desired degree of curvature.

The appearance of big dimer rings in Figure 19 for K ring also corroborates the above observation. That is, even for structure of increased rigidity like K ring, the DNA helix bundle can still find ways to break free of the enforced degree of curvature, becoming more open than originally designed.

4.2.4.2 Severe deformation in V ring

For V ring, a large percentage of the observed particles do not resemble a curvature but are severely deformed, signifying significant folding problem. Again, this could be attributed to the deviation from crossover spacing rules.

5 Conclusion

The set of design principles for curvature outlined herein has brought significant yield and structure improvement in curvature assembly, as shown in the comparison between K ring, which strictly conforms to those principles, and A ring, one found in literature.

Arguably, the above conclusion is not yet definitive considering that A ring and K ring, besides their difference in length gradients, which is hypothesized to be responsible for the distinct degrees of curvature, also differ in cross-sections, crossover patterns, helix lengths, and torsional rigidity. Naturally, controlling these additional factors will yield a more definitive conclusion, yet the cost of staples synthesis for each origami structure, which hovers around 1000 euros as of August 2018, renders that prohibitive within the scope of this thesis.

Experimental observation also shows the limitation of the geometry-based approach in predicting degree of curvature for structures with low cross-sectional rigidity via the example of open A ring. This also hints at the importance of rigidity in enforcing curvature.

Another main objective of the thesis is designing a square-lattice-based ring using the same principles, which was met with limited success. Albeit some exemplary particles were found, their prevalence was very low, and could not be effectively separated from defect species even with the most selective methods of purification, e.g., gel electrophoresis. Nevertheless, this is already anticipated considering the design's extreme number of bps/turn after modification, a limitation that presumably could be circumvent by either (1) returning the number of bps/turn to its normal value by increase helix length, which is only suitable for rings of large diameters, or (2) adopting the off-lattice approach. This further highlights the importance of crossover spacing rules in designing complex DNA origami structures.

In assessing assembly quality, this thesis relied on TEM and subjective evaluation of particle structures, which could be biased since TEM images are taken after particles were deposited on a flat surface. These shortcomings can be remedied by adopting a more quantitative assessment of origami structures assembly [39].

Overall, the logical next step would be to implement the off-lattice approach to design a ring with a complex, sufficiently rigid cross-section, and a low radius of curvature which could not be achieved with high yield using the on-lattice approach [8].

References

[1] N. C. Seeman, “DNA in a material world,” *Nature*, vol. 421, no. 6921, pp. 427–431, Jan. 2003.

[2] G. A. Ozin *et al.*, “Nanofabrication by self-assembly,” *Materials Today*, vol. 12, no. 5, pp. 12–23, May 2009.

[3] P. Wang, T. A. Meyer, V. Pan, P. K. Dutta, and Y. Ke, “The Beauty and Utility of DNA Origami,” *Chem*, vol. 2, no. 3, pp. 359–382, Mar. 2017.

[4] P. W. K. Rothemund, “Folding DNA to create nanoscale shapes and patterns,” *Nature*, vol. 440, no. 7082, pp. 297–302, Mar. 2006.

[5] S. M. Douglas, A. H. Marblestone, S. Teerapittayanon, A. Vazquez, G. M. Church, and W. M. Shih, “Rapid prototyping of 3D DNA-origami shapes with caDNAno,” *Nucleic Acids Research*, vol. 37, no. 15, pp. 5001–5006, Aug. 2009.

[6] C. E. Castro *et al.*, “A primer to scaffolded DNA origami,” *Nature Methods*, vol. 8, no. 3, pp. 221–229, Mar. 2011.

[7] P. D. E. Fisher *et al.*, “A Programmable DNA Origami Platform for Organizing Intrinsically Disordered Nucleoporins within Nanopore Confinement,” *ACS Nano*, vol. 12, no. 2, pp. 1508–1518, Feb. 2018.

[8] H. Dietz, S. M. Douglas, and W. M. Shih, “Folding DNA into Twisted and Curved Nanoscale Shapes,” *Science*, vol. 325, no. 5941, pp. 725–730, Aug. 2009.

[9] D. Han, S. Pal, J. Nangreave, Z. Deng, Y. Liu, and H. Yan, “DNA Origami with Complex Curvatures in Three-Dimensional Space,” *Science*, vol. 332, no. 6027, pp. 342–346, Apr. 2011.

[10] Y. Yang *et al.*, “Self-assembly of size-controlled liposomes on DNA nanotemplates,” *Nature Chemistry*, vol. 8, no. 5, pp. 476–483, May 2016.

[11] P. Ketterer *et al.*, “DNA origami scaffold for studying intrinsically disordered proteins of the nuclear pore complex,” *Nature Communications*, vol. 9, no. 1, p. 902, Mar. 2018.

[12] E.-M. Roller, L. K. Khorashad, M. Fedoruk, R. Schreiber, A. O. Govorov, and T. Liedl, “DNA-Assembled Nanoparticle Rings Exhibit Electric and Magnetic Resonances at Visible Frequencies,” *Nano Lett*, vol. 15, no. 2, pp. 1368–1373, Feb. 2015.

[13] W. Xu *et al.*, “A programmable DNA origami platform to organize SNAREs for membrane fusion,” *J Am Chem Soc*, vol. 138, no. 13, pp. 4439–4447, Apr. 2016.

[14] H. G. Franquelim, A. Khmelinskaia, J.-P. Sobczak, H. Dietz, and P. Schwille, “Membrane sculpting by curved DNA origami scaffolds,” *Nature Communications*, vol. 9, no. 1, p. 811, Feb. 2018.

[15] M. J. Urban *et al.*, “Plasmonic Toroidal Metamolecules Assembled by DNA Origami,” *J. Am. Chem. Soc.*, vol. 138, no. 17, pp. 5495–5498, May 2016.

[16] Y. Ke *et al.*, “Multilayer DNA Origami Packed on a Square Lattice,” *J Am Chem Soc*, vol. 131, no. 43, p. 15903, Nov. 2009.

[17] B. Alberts, A. Johnson, J. Lewis, M. Raff, K. Roberts, and P. Walter, “The Structure and Function of DNA,” *Molecular Biology of the Cell. 4th edition*, 2002.

[18] G. Banfalvi, “Structural organization of DNA,” *Biochemical Education*, vol. 14, no. 2, pp. 50–59, Apr. 1986.

[19] C. F. Matta, N. Castillo, and R. J. Boyd, “Extended Weak Bonding Interactions in DNA: π-Stacking (Base−Base), Base−Backbone, and Backbone−Backbone Interactions,” *J. Phys. Chem. B*, vol. 110, no. 1, pp. 563–578, Jan. 2006.

[20] D. W. Ussery, “DNA Structure: A-, B- and Z-DNA Helix Families,” in *eLS*, American Cancer Society, 2002.

[21] D. Svozil, J. Kalina, M. Omelka, and B. Schneider, “DNA conformations and their sequence preferences,” *Nucleic Acids Research*, vol. 36, no. 11, pp. 3690–3706, Jun. 2008.

[22] M. Bansal, “DNA structure: revisiting the Watson-Crick double helix,” *Current Science*, vol. 85, pp. 1556–1563, Dec. 2003.

[23] L. Pray, “Discovery of DNA Double Helix: Watson and Crick,” *Nature Education*, 2008. [Online]. Available: https://www.nature.com/scitable/topicpage/discovery-of-dna-structure-and-function-watson-397. [Accessed: 10-Nov-2018].

[24] S. Harteis and S. Schneider, “Making the Bend: DNA Tertiary Structure and Protein-DNA Interactions,” *Int J Mol Sci*, vol. 15, no. 7, pp. 12335–12363, Jul. 2014.

[25] C. J. Kearney, C. R. Lucas, F. J. O’Brien, and C. E. Castro, “DNA Origami: Folded DNA-Nanodevices That Can Direct and Interpret Cell Behavior,” *Adv Mater*, vol. 28, no. 27, pp. 5509–5524, Jul. 2016.

[26] S. M. Douglas, H. Dietz, T. Liedl, B. Högberg, F. Graf, and W. M. Shih, "Self-assembly of DNA into nanoscale three-dimensional shapes," *Nature*, vol. 459, no. 7245, pp. 414–418, May 2009.

[27] Y. Ke, J. Sharma, M. Liu, K. Jahn, Y. Liu, and H. Yan, "Scaffolded DNA Origami of a DNA Tetrahedron Molecular Container," *Nano Lett.*, vol. 9, no. 6, pp. 2445–2447, Jun. 2009.

[28] E. S. Andersen *et al.*, "Self-assembly of a nanoscale DNA box with a controllable lid," *Nature*, vol. 459, no. 7243, pp. 73–76, May 2009.

[29] R. V. Reshetnikov *et al.*, "A coarse-grained model for DNA origami," *Nucleic Acids Res.*, vol. 46, no. 3, pp. 1102–1112, Feb. 2018.

[30] E. A. Hemmig *et al.*, "Optical Voltage Sensing Using DNA Origami," *Nano Lett.*, vol. 18, no. 3, pp. 1962–1971, Mar. 2018.

[31] Y. Ke, G. Bellot, N. V. Voigt, E. Fradkov, and W. M. Shih, "Two design strategies for enhancement of multilayer–DNA-origami folding: underwinding for specific intercalator rescue and staple-break positioning," *Chem. Sci.*, vol. 3, no. 8, pp. 2587–2597, Jul. 2012.

[32] Y. Ke *et al.*, "Multilayer DNA Origami Packed on a Square Lattice," *Journal of the American Chemical Society*, vol. 131, no. 43, pp. 15903–15908, Nov. 2009.

[33] I. H. Stein, V. Schüller, P. Böhm, P. Tinnefeld, and T. Liedl, "Single-Molecule FRET Ruler Based on Rigid DNA Origami Blocks," *ChemPhysChem*, vol. 12, no. 3, pp. 689–695, Feb. 2011.

[34] D.-N. Kim, F. Kilchherr, H. Dietz, and M. Bathe, "Quantitative prediction of 3D solution shape and flexibility of nucleic acid nanostructures," *Nucleic Acids Research*, vol. 40, no. 7, pp. 2862–2868, Apr. 2012.

[35] B. Kick, F. Praetorius, H. Dietz, and D. Weuster-Botz, "Efficient Production of Single-Stranded Phage DNA as Scaffolds for DNA Origami," *Nano Lett.*, vol. 15, no. 7, pp. 4672–4676, Jul. 2015.

[36] K. F. Wagenbauer *et al.*, "How We Make DNA Origami," *Chembiochem*, vol. 18, no. 19, pp. 1873–1885, 05 2017.

[37] E. Stahl, T. G. Martin, F. Praetorius, and H. Dietz, "Facile and Scalable Preparation of Pure and Dense DNA Origami Solutions," *Angewandte Chemie International Edition*, vol. 53, no. 47, pp. 12735–12740, Nov. 2014.

[38] T. G. Martin and H. Dietz, "Magnesium-free self-assembly of multi-layer DNA objects," *Nature Communications*, vol. 3, p. 1103, Oct. 2012.

[39] K. F. Wagenbauer, C. H. Wachauf, and H. Dietz, "Quantifying quality in DNA self-assembly," *Nature Communications*, vol. 5, no. 1, Dec. 2014.

Appendices

APPENDIX 1. CaDNAno design for VRing

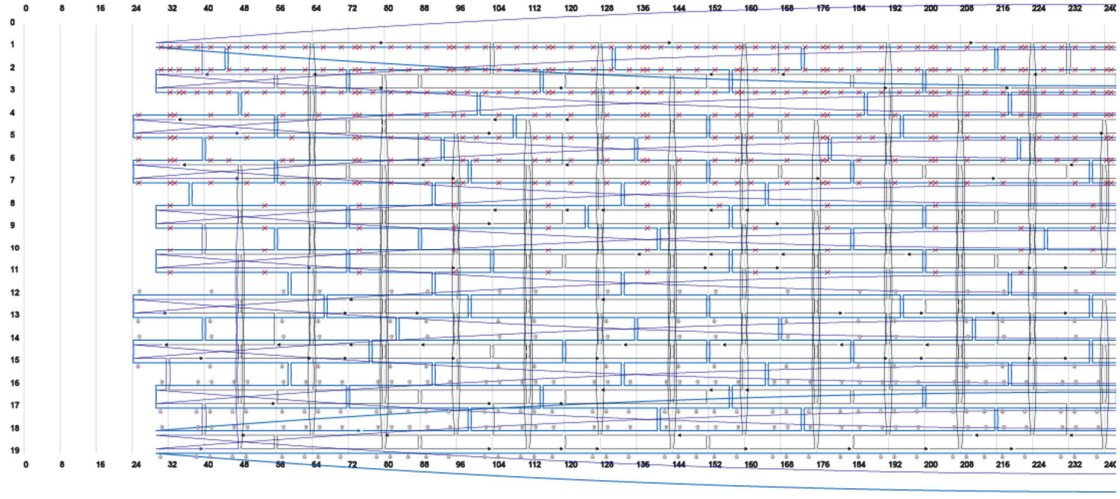

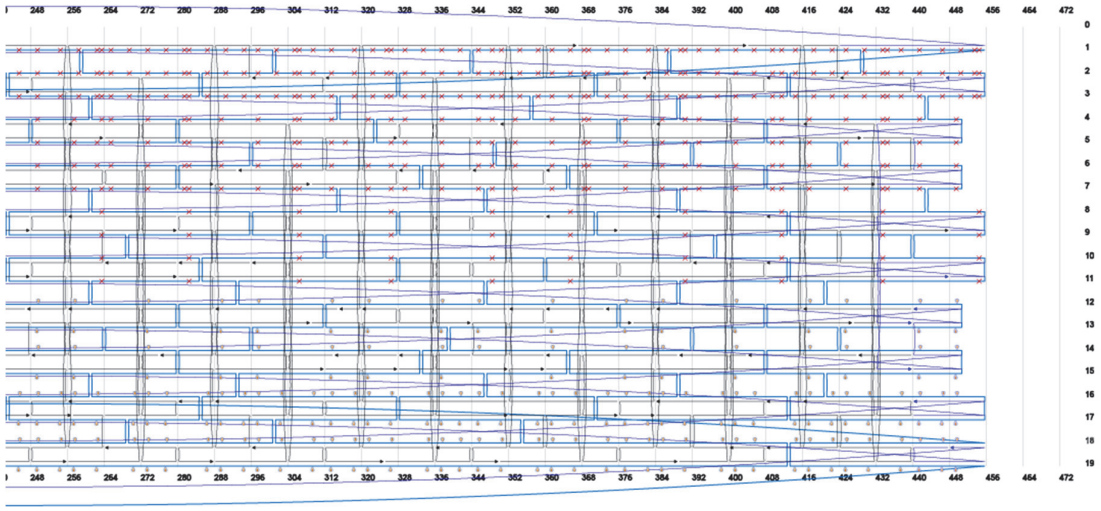

APPENDIX 2. CaDNAno design for KRing

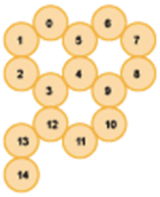

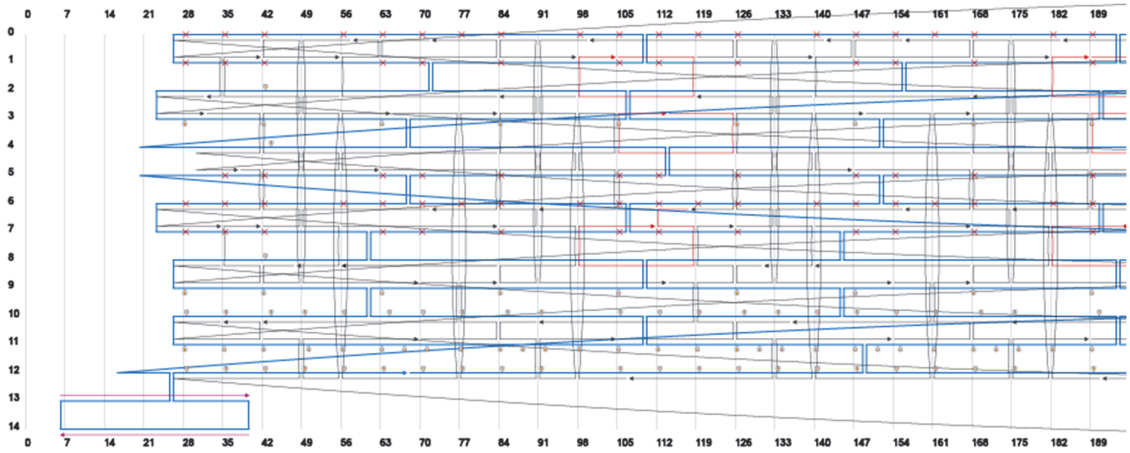

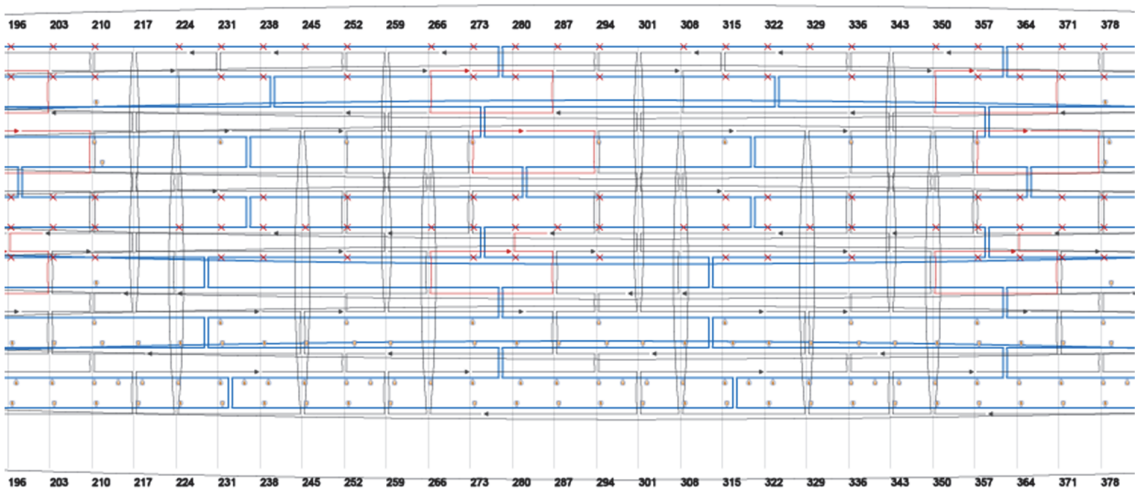

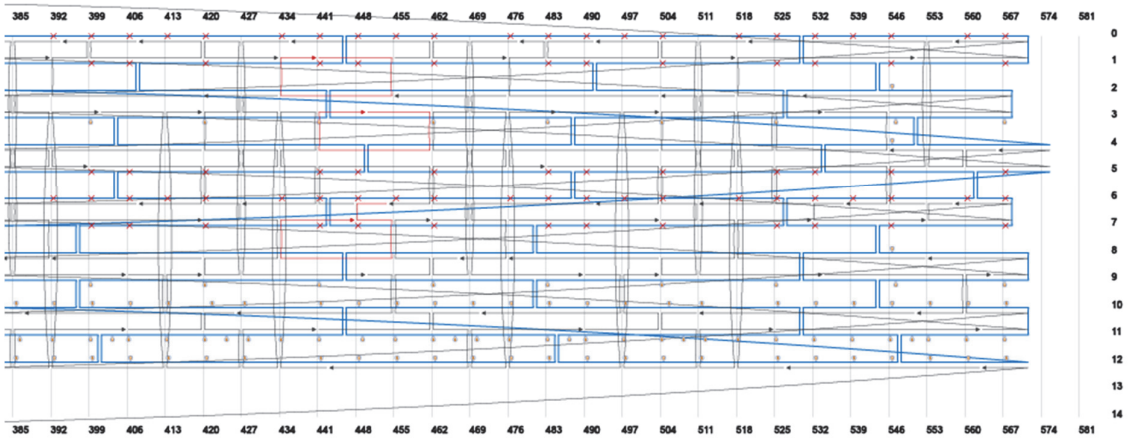

APPENDIX 3. CaDNAno design for ARing

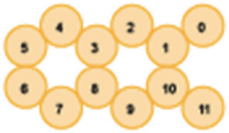

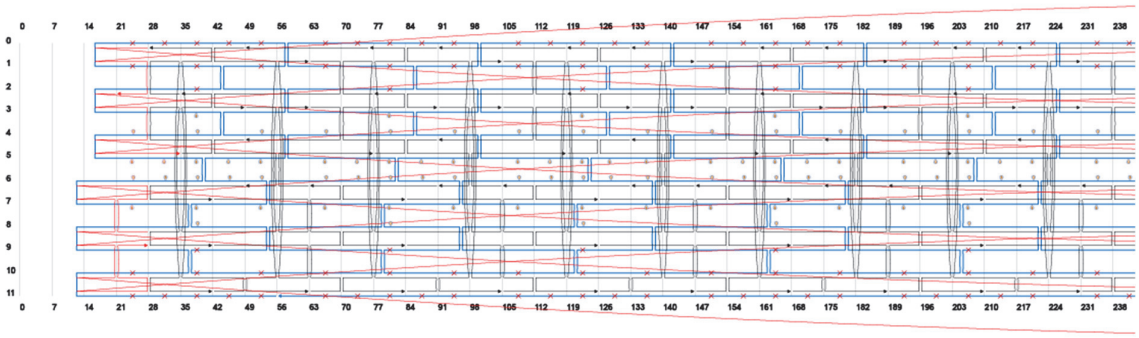

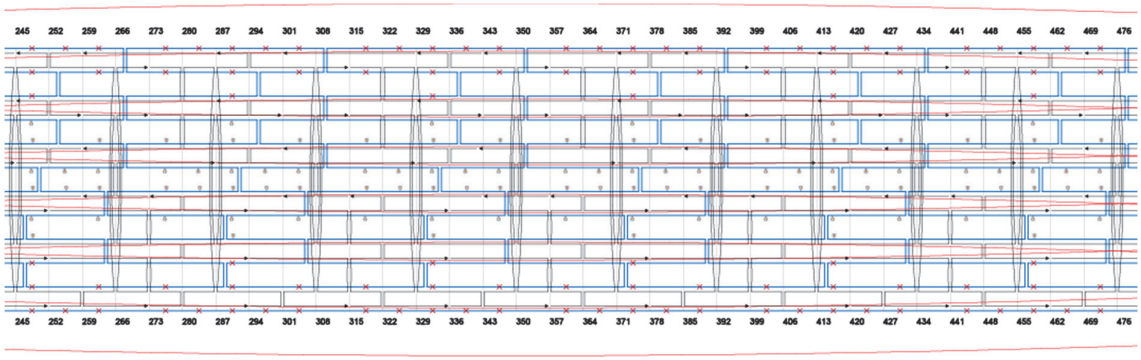

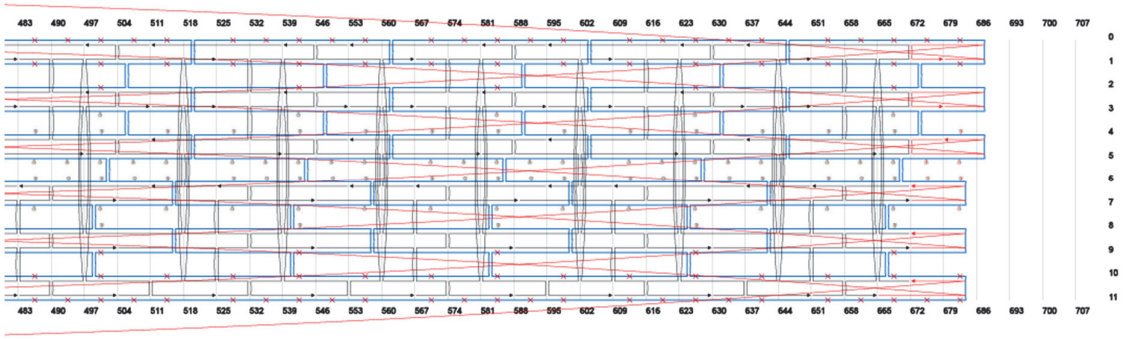

APPENDIX 4. CaDNAno design for open ARing